Optimizing a CRISPR-Cas13d gene circuit for tunable target RNA downregulation with minimal collateral RNA cutting

Yiming Wan[1], Damiano Coraci[2], Christopher Helenek[1,2], Gábor Balázsi[1,2,3,*]

[1]The Louis and Beatrice Laufer Center for Physical and Quantitative Biology, Stony Brook University, Stony Brook, NY 11794, USA

[2]Department of Biomedical Engineering, Stony Brook University, Stony Brook, NY 11794, USA

[3]Stony Brook Cancer Center, Stony Brook University, Stony Brook, NY 11794, USA

[*]**Corresponding author:**

Gábor Balázsi, Ph.D.
Henry Laufer Professor
Laufer Center for Physical & Quantitative Biology
Department of Biomedical Engineering
115C Laufer Center, Z-5252
Stony Brook University
Stony Brook, NY 11794
Tel. +1-631-632-5414;
Email: gabor.balazsi@stonybrook.edu
ORCID: 0000-0002-6865-5818

SUMMARY

The invention of RNA-guided DNA cutting systems has revolutionized biotechnology. More recently, RNA-guided RNA cutting by Cas13d entered the scene as a highly promising alternative to RNA interference to engineer cellular transcriptomes for biotechnological and therapeutic purposes. Unfortunately, "collateral damage" by indiscriminate off-target cutting tampered enthusiasm for these systems. Yet, how collateral damage, or even RNA target reduction depends on Cas13d and guide RNA abundance has remained unclear due to the lack of expression-tuning studies to address this question. Here we use precise expression-tuning gene circuits to show that target RNA reduction depends sensitively on both Cas13d and guide RNA levels, part of which might result from collateral damage of Cas13d complexes activated by target cutting. Using RNA-level control techniques, we develop new Multi-Level Optimized Negative-Autoregulated Cas13d and crRNA Hybrid (MONARCH) gene circuits that achieve a high dynamic range of target reduction while minimizing basal target cutting and collateral damage in human kidney cells and green monkey cells most frequently used in human virology. MONARCH systems should bring RNA-guided RNA cutting systems to the forefront, as easily applicable, programmable tools for transcriptome engineering in biotechnological and medical applications.

Keywords:

Cas13d, RNA-targeting, CRISPR, synthetic gene circuit, collateral damage, downregulation

INTRODUCTION

The discovery of CRISPR ("clustered regularly interspaced short palindromic repeats") systems[1-4] has revolutionized biotechnology. The use of various CRISPR-associated (Cas) proteins has facilitated relatively straightforward deletion, insertion, and editing of genes, enabling extensive control and study across bacterial, fungal, plant, and mammalian cells[4-6]. Yet, gene expression levels are as critical as protein-coding sequences in determining cellular phenotypes[7-11]. To manipulate gene expression without altering DNA sequences, enzymatically dead Cas (dCas) proteins, fused with silencing and activator domains, were developed[12]. However, these dCas systems, which control gene expression through DNA binding, may lead to nonspecific binding, spread of chromatin modifications, and diversion of cellular resources, which are undesirable side effects[13-16]. Recently, RNA-targeting CRISPR systems have emerged as promising alternatives that address these issues by programmable cutting of mRNA instead of DNA[17]. Nonetheless, challenges such as nonspecific, off-target RNA cutting ("collateral damage") have moderated the enthusiasm for these novel systems[18,19]. Despite these drawbacks, Cas13d represents a potentially crucial, modular, targetable, and programmable alternative to existing RNA interference technologies, promising significant advancements in both research and clinical settings.

Despite considerable information on Cas13d, how its on-target and off-target activities depend on Cas13d and crRNA expression levels remains poorly understood. Consequently, it is currently unknown whether adjusting the relative expression levels of Cas13d and crRNA could reduce or eliminate collateral damage. This gap in knowledge is due to a lack of employing genetic systems to fine-tune the expression of Cas13d and crRNA. Current studies typically rely on binary on/off approaches or crRNA mismatches[20,21], which do not allow for temporal adjustments of control over the same cells.

Over the past two decades, we have developed and refined negative feedback (NF) based synthetic gene circuits for precise gene expression tuning[22-25]. These gene circuits have been applied in yeast[22], and then developed into mammalian NF (mNF) gene circuits in Chinese hamster[26,27], and human cells[23,24,28], revealing surprising phenotypic effects associated with fine-tuned gene expression changes. For instance, using an mNF system to fine-tune metastasis regulator BACH1 expression, we discovered an unexpected non-monotone relationship between its expression and cellular invasion[28]. However, mNF gene circuits have not yet been applied to modulate the components of Cas13d or other CRISPR systems. Thus, there is a significant opportunity to leverage existing synthetic gene-regulatory technologies to enhance the specificity and efficacy of CRISPR-based gene editing tools, particularly to enable precise fine-tuning of RNA downregulation with novel CRISPR-Cas13d gene circuits.

In this study, we initially developed a traditional mNF-Cas13d gene circuit that transcriptionally tunes the expression of Cas13d to facilitate dose-dependent target reduction in Human Embryonic Kidney (HEK 293) cells. Despite the broad dynamic range of Cas13d tuning, excessive on-target activity of the Cas13d:crRNA complex caused substantial basal target reduction even without mNF-Cas13d induction, restricting the dynamic range of target downregulation. Furthermore, joint Cas13d and crRNA expression also depleted non-target reporter RNAs, indicating considerable collateral damage. To address these limitations, we

developed a novel gene circuit design, termed Multi-Level Optimized Negative-Autoregulated Cas13d and crRNA Hybrid (MONARCH). This design utilizes the inherent ability of Cas13d to process its own crRNA as a mechanism for RNA-level autoregulation, effectively attenuating the expression of both Cas13d and crRNA. Besides nearly eliminating collateral damage, MONARCH achieved a broad dynamic range of target downregulation by minimal basal cutting and robust knockdown efficacy of both transient and stable RNA targets upon induction. We further optimized MONARCH by incorporating an mRNA stabilizing Triplex motif, to enable even broader on-target dynamic range without introducing collateral damage. Finally, we demonstrated MONARCH's functionality in Vero E6 green monkey kidney cells, the workhorse of human virology, offering a scalable and versatile cellular platform for quantitative RNA-targeting in antiviral studies and therapeutic development.

RESULTS

A versatile landing-pad cellular platform enables rapid and reliable synthetic gene circuit integration

To downregulate arbitrary mRNA targets, we set out to precisely tune Cas13d expression using the mNF gene circuit[23]. Thus, we inserted the gene encoding Cas13d as the last component in a multi-gene construct that also contains hTetR and the reporter mCherry. We used D2i, a CMV-derived promoter with TetO2 binding sites to drive the expression of this mNF-hTetR-mCherry-Cas13 construct, ensuring negative autoregulation by TetR. The expression of all gene circuit components is precisely tunable by adding Doxycycline to the growth medium. Doxycycline diffuses into cells, binds hTetR and prevents its DNA binding, elevating mNF-Cas13d expression. Negative autoregulation reduces expression noise for all genes up until saturation, ensuring precise Cas13d gene expression tuning.

To rigorously assess the efficacy of dose-dependent RNA downregulation by the chromosomally integrated mNF-Cas13d gene circuit, we utilized a genomic integration platform we recently established in HEK293 cells[28]. This platform overcomes major drawbacks of widely used viral and CRISPR-Cas9 based genomic integration methods by utilizing a Landing Pad (LP), which is a set of selection markers and the GFP reporter flanked by a pair of heterologous Flp-recombinase targeting sites. We incorporated the LP into the AAVS1 safe harbor site (SHS) of the human genome using CRISPR-Cas9-mediated target insertion **(Figure 1A)**. Once established, the LP allows site-specific integration of any desired DNA payload into the AAVS1 site through Flp-recombinase-mediated cassette exchange (FLP-RMCE).

Using HEK293-LP cells, we integrated the mNF-Cas13d synthetic gene circuit by FLP-RMCE, replacing the original LP cassette with the mNF-Cas13d gene circuit and new selection markers **(Figure 1B)**. The mCherry reporter in the mNF-Cas13d gene circuit indicated some basal expression even without doxycycline (Dox) induction **(Figure 1C)**. Fluorescence shifting from green to red in the surviving cell population indicated successful cassette switching via RMCE **(Figure 1B)**.

To evaluate the performance of the integrated mNF-Cas13d gene circuit, we monitored the expression levels and variability (coefficient of variation, CV) of mCherry reporter expression under constant Dox concentrations ranging from 0 to 100 ng/ml, 72 hours post-induction. We observed a gradual, monotonic increase in mCherry expression as indicated by flow cytometry histograms **(Figure 1D)**. The dose-response of mCherry to Dox, validated through three independent replicates, indicated a 14-fold change between maximum and basal levels **(Figure 1E)**. Additionally, the CV of mCherry expression remained consistently low, with only a slight increase at higher Dox concentrations **(Figure 1F)**, indicating stable, low-noise characteristics as previously reported in other mNF gene circuits tuning the expression of other genes[26,28-30].

The mNF-Cas13d gene circuit achieves dose-dependent target mRNA reduction but with substantial basal target downregulation

To assess the tunability of RNA target reduction by the integrated mNF-Cas13d gene circuit, we constructed a single-plasmid template to co-express a BFP reporter with either non-targeting crRNA or BFP-targeting crRNA **(Figure S1A)**. Additionally, to determine the maximum target reduction achievable by the gene circuit, we engineered and integrated a feedback-disabled Cas13d expression cascade that lacked the TetO2 sites in the CMV promoter but retained the

same coding sequence as the mNF-circuit **(Figure S1A)**. We either pre-induced or kept uninduced (Dox; 100 or 0 ng/ml) both engineered cell lines for 72 hours, after which we transfected them with the plasmids containing either BFP-targeting or non-targeting crRNA along with the BFP reporter, maintaining Dox unchanged. Flow cytometry results 72 hours post-transfection indicated tunability of RNA downregulation solely with the intact mNF-Cas13d gene circuit, which at full induction achieved knockdown levels comparable to those of its constitutive counterpart **(Figure S1B)**. However, we observed significant (>60%) basal target downregulation even without induction, raising concerns about the applicability of the gene circuit.

To mitigate this pronounced basal target reduction, we tried to reduce target expression, hypothesizing that transiently transfected BFP, expressed from the strong EF1α promoter, might exaggerate basal target reduction. We reevaluated inducible RNA knockdown efficiency by the mNF-Cas13d gene circuit using similarly cloned single-plasmid templates with BFP expressed from the weaker SV40 promoter **(Figure 2A)**. Following the same transfection protocol resulted in a dose-dependent reduction in BFP, corresponding to the dose-responsive increase of mCherry expression from the gene circuit **(Figure 2B-C)**. However, the basal target reduction still remained substantial (>40%), significantly limiting the dynamic range of downregulation (only approximately 25% difference from basal to maximum induction).

To address this basal target reduction issue, we considered regulating crRNA levels as a potential strategy, as opposed to the typical constitutive crRNA expression. We replaced the constitutive hU6 promoter, originally used for crRNA expression, with a modified hU6-2O incorporating TetO2 sited[31] (hU6-2O), to allow repression by hTetR. Initial tests with both mNF-Cas13d and constitutive CMV-Cas13d cells, with the strong EF1α promoter driving BFP target expression **(Figure S1C)**, indicated inducible RNA downregulation, with significantly diminished basal target reduction from over 60% to about 40%, while the maximum expression's reduction decreased only moderately from over 80% to about 75% **(Figure S1D)**. Furthermore, lowering BFP target expression diminished basal target reduction (from over 40% to about 25%) while increasing the dynamic range of RNA downregulation (from 25% to 40% inducible reduction), corresponding to dose-responsive mCherry increase from the gene circuit **(Figure 2D-F)**.

To test the effect of genomic target integration, we subsequently evaluated the dose-responses of targeting a stably expressed genomic target using the mNF-Cas13d gene circuit. We constructed an all-in-one testing platform containing the mNF-Cas13d gene circuit, a target GFP expressed from the SV40 promoter, and GFP-targeting crRNA expressed from the hU6-2O promoter, with a non-targeting crRNA as control **(Figure 2G)**. We observed appropriate mCherry dose-responses from both integrated constructs with similar dynamic ranges **(Figure 2H)**, and a dose-dependent GFP downregulation up to 80%, although a 40% basal target reduction still persisted **(Figure 2I)**.

Overall, we showed that the mNF-Cas13d gene circuit can achieve dose-dependent target RNA downregulation. However, the circuit exhibited severe basal target downregulation even without induction, associated with both Cas13d and crRNA expression, indicating the necessity of further optimization for broader applicability.

The activated Cas13d:crRNA complex causes severe collateral off-target reduction

In all experiments so far, we consistently observed a significant reduction of mCherry expression in cells transfected with targeting crRNA compared to those with non-targeting

crRNA at higher induction **(Figure 2 B, E, H)**. This raised concerns about potential collateral damage by the activated Cas13d:crRNA complex. Previous studies have noted Cas13d's collateral, off-target RNase activity when cutting overexpressed targets, highly repetitive targets, and even sufficiently abundant endogenous transcripts[18,32,33], with variations potentially dependent on cell type[19] but evidenced in both HeLa and HEK293 cells[33]. Therefore, we aimed to evaluate the extent of collateral RNA-cutting damage introduced by the mNF-Cas13d gene circuit, which might underlie the strong basal target downregulation we observed, especially at higher induction.

To examine collateral damage, we repurposed the single-plasmid template to include a regulated GFP-targeting crRNA while co-expressing an orthogonal, non-target BFP reporter. Initially, to demonstrate the existence of collateral damage, we expressed BFP at moderate levels using the SV40 promoter while maximizing GFP target expression with the CMV promoter, to boost up activated Cas13d:crRNA complexes **(Figure S2A)**. Upon co-transfection into mNF-Cas13d cells, mCherry expression consistently decreased at both 1 and 10 ng/ml Dox induction **(Figure S2B)**, alongside a dose-dependent GFP target reduction with substantial basal effect **(Figure S2C)**, and a concurrent dose-dependent reduction in BFP, indicating Cas13d's collateral RNase activity **(Figure S2D)**.

In actual biological contexts, the abundance of a specific target RNA is only a fraction of the total RNA pool. Therefore, to further assess collateral damage in more realistic scenarios, we modified the single-plasmid template to express the non-target BFP reporter under the strong EF1α promoter, while the GFP target was expressed from the SV40 promoter **(Figure 3A)**. Similarly, we observed dose-dependent GFP on-target reduction correlating with increases in mCherry levels **(Figure 3B-C)**. However, the dose-dependent reduction in BFP was even more pronounced, and exacerbated by unregulated crRNA expression **(Figure 3D)**, suggesting that targeting RNA with many activated Cas13d:crRNA complexes can result in stronger off-target effects due to global collateral damage.

To evaluate the impact of such collateral damage on cell viability, we reused the single-plasmid assay with SV40 expressing BFP and hTetR-regulated, BFP-targeting crRNA to define a reasonable scale of conditions for collateral damage in cells **(Figure S2E)**. Our initial results indicated that Cas13d expression alone, with non-targeting crRNA, did not significantly impact cell viability, confirming that activation of Cas13d:crRNA complexes is necessary for the observed effects **(Figure S2F)**. However, when transfected with on-target crRNA, we noted a dose-dependent decrease in cell viability with increased Cas13d and crRNA expression, especially at higher induction **(Figure S2G)**, while the viability of cells transfected with non-targeting crRNA was practically unaffected.

Finally, to mimic a realistic scenario where the mNF-Cas13d gene circuit is intended to downregulate specific gene targets near non-target genes in the genome, we constructed an extended all-in-one testing platform containing the mNF-Cas13d gene circuit, GFP expressed from the SV40 promoter, GFP-targeting crRNA from the hU6-2O promoter, and a non-target BFP reporter also expressed from the SV40 promoter, with a non-targeting crRNA as control **(Figure 3E)**. The mCherry dose-responses were consistent with previous findings, from both target and control constructs, with similar dynamic ranges and a drop in mCherry expression at higher induction **(Figure 3F)**, a consistent dose-dependent GFP on-target downregulation up to 80%, with a 40% basal target reduction still persisting **(Figure 3G)**, and a corresponding dose-

dependent reduction in BFP levels, especially at higher induction where substantial Cas13d and crRNA were expressed and activated in cells **(Figure 3H)**.

Collectively, these results provide strong evidence for substantial collateral damage when employing Cas13d to degrade sufficiently abundant RNA targets in cells, a challenge that must be carefully resolved before broad application in biological research and therapeutic development. However, it appears that the current mNF gene circuit design is insufficient to address this issue, and further optimization will be necessary.

Multi-level negative autoregulation of both Cas13d and crRNA reduces collateral damage and improves on-target dynamic range

Given the high efficacy of RNA degradation by the Cas13d:crRNA complex at relatively low expression levels, we hypothesized that the key to reducing collateral damage and improving the dynamic range of on-target activity was to induce both Cas13d and crRNA expression within a lower range compared to traditional mNF circuits. Inspired by a previous study that utilized Cas13d's crRNA processing capability as a mechanism for RNA-level negative autoregulation[33], we incorporated a pre-crRNA motif into the 3'UTR of the mNF coding region before the poly(A) signal. This innovation led to the design of a multi-level optimized negative-autoregulated Cas13d and crRNA hybrid circuit, termed MONARCH **(Figure 4A)**.

The MONARCH 1.0 system achieves transcriptional repression through TetR binding to TetO2 sites at the promoter region, while the expression of Cas13d results in accelerated degradation of its own mRNA, due to eliminating the poly(A) signal when processing the crRNA located in the 3'UTR. This design lowers expression levels at each induction dosage and thus reduces basal target reduction by lowering both Cas13d and crRNA expression **(Figure 4A)**. To characterize the performance of this new gene circuit, we integrated MONARCH 1.0 into the AAVS1 site in HEK 293 LP parental cells using the same RMCE strategy. Upon Dox induction, mCherry level increased in a Dox dose-responsive manner as evidenced by histogram shifts and fluorescence quantitation **(Figures 4B-C)**, while preserving the low-noise expression profile characteristic of mNF gene circuits **(Figure 4D)**. However, the total tunability of Cas13d expression was significantly reduced compared to traditional mNF circuits, as expected due to stronger RNA-level regulation at higher dosages **(Figure 4B)**.

To determine whether collateral damage still persists in the MONARCH 1.0 system, we retested the cells by co-transfecting them with an abundant GFP target and a moderate non-target BFP reporter **(Figure S3A)**. Compared to the mNF-Cas13d gene circuit with non-targeting crRNA control, we observed significantly lower levels of mCherry expression **(Figure S3B)**, even lower basal target reduction than for the regulated crRNA strategy (20% vs. 30%), and appropriate dose-dependent GFP reduction **(Figure S3C)**, along with a significant reduction in collateral damage as evidenced by negligible changes in BFP expression **(Figure S3D)**. These results indicated that the MONARCH 1.0 system effectively reduces unwanted collateral damage while preserving dose-dependent on-target activity with even lower basal target reduction.

Furthermore, we assessed the dose-dependent downregulation of RNA expressed from stably LP-integrated targets with MONARCH 1.0, as well as the level of collateral damage. Thus, we introduced to non-target genes with a stably chromosomally integrated all-in-one testing platform for the MONARCH 1.0 system **(Figure 4E and Figure S3E)**. We observed a low dynamic range of mCherry expression with Dox induction, indicating a highly reduced level of Cas13d and crRNA in cells **(Figures 4F and Figure S3F)**, and a consistent low-noise profile of

such inducible expression **(Figures 4G and Figure S3G)**. Compared to basal constructs, the basal on-target reduction dropped to only 3-5% when targeting a stable gene target in the genome, while the maximum on-target reduction reached about 50% from the basal, indicating an improved on-target dynamic range (from 40% to about 50%) **(Figures 4H and Figure S3H)**. GFP-target expression variation remained low, suggesting homogeneous RNA degradation across the cell population rather than variable degradation in subsets of cells **(Figure 4I)**. Additionally, we observed no detectable collateral damage to the non-target BFP reporter while targeting GFP dose-dependently **(Figure S3I)**.

Finally, after demonstrating precise on-target downregulation with the MONARCH 1.0 system, we tested it on an actual endogenous gene target, BACH1, an important metastatic regulator in breast cancer cells[28,34]. By combining multiple crRNAs and transiently transfecting them into MONARCH 1.0 cells **(Figure 4J)**, we observed no basal target reduction from uninduced MONARCH 1.0 and a gradual reduction in BACH1 mRNA (up to 50% from the basal) with increasing Dox induction **(Figure 4K)**. This demonstrated the potential of the MONARCH system to achieve precise and effective target RNA downregulation, even transiently.

Overall, we have introduced a novel circuit design that leverages multi-level negative autoregulation on Cas13d and crRNA to simultaneously reduce collateral damage and improve on-target activity characteristics. The MONARCH system's capability to achieve tunable RNA downregulation for both transient and stable targets will offer significant potential for quantitative genetic studies and therapeutic development.

MONARCH system optimization further improves on-target activity while preserving minimal collateral damage

We have demonstrated that MONARCH 1.0 could retain dose-dependent target RNA downregulation without detectable collateral damage. However, we considered the maximum target reduction of up to 50% unsatisfying, which could be worse if the native target abundance was lower compared to SV40-driven expression or endogenous BACH1 expression. Therefore, we decided to optimize the MONARCH system to improve its on-target activity, especially at higher induction levels, without reintroducing collateral damage. We hypothesized that the MONARCH 1.0 system may have lowered Cas13d and crRNA expression too much and elevating them slightly could effectively improve on-target activity without significant collateral damage. Thus, we designed MONARCH 2.0, an improved multi-level optimized negative-autoregulated Cas13d and crRNA hybrid circuit **(Figure 5A)**.

Similar to MONARCH 1.0 in action, MONARCH 2.0 still had both TetR-TetO2-based transcriptional regulation and crRNA-processing-based RNA-level regulation. However, we incorporated Triplex, an additional RNA structural motif between the coding region and pre-crRNA motif. Triplex is a 110-nt structure derived from the 3′ end of the mouse non-coding RNA Metastasis-associated lung adenocarcinoma transcript 1 (Malat1), previously described to stabilize transcripts lacking poly(A) tails through the formation of a tertiary structure[34]. It has been successfully used to incorporate CRISPR-Cas12a and its guide RNA into a single transcript[35]. Here, we similarly applied it to enable better Cas13d expression with crRNA in the same transcript **(Figure 5A)**.

To characterize the performance of MONARCH 2.0, we integrated MONARCH 2.0 into the AAVS1 site in HEK 293 LP parental cells using the same RMCE strategy. Upon Dox induction, histogram shifts and fluorescence quantitation indicated significantly improved dose-responsive

tuning of mCherry levels **(Figures 5B-C)**, while preserving a low-noise expression profile throughout **(Figure 5D)**. with MONARCH 2.0, Cas13d expression was tunable over a 7-fold dynamic range, with basal target reduction comparable to MONARCH 1.0, but significantly higher maximal expression levels at full induction **(Figure 4B)**.

To determine whether the MONARCH 2.0 system would reintroduce collateral damage, we similarly tested the cells by co-transfecting them with an abundant GFP target and a moderate non-target BFP reporter **(Figure S4A)**. First, compared to the mNF-Cas13d gene circuit with non-targeting crRNA control, we still observed significantly lower levels of mCherry expression **(Figure S4B)**, comparably low basal target downregulation without induction as for MONARCH 1.0, and improved dose-dependent GFP reduction **(Figure S4C)**, along with a slight increase of collateral damage only at the highest induction dosage as evidenced by 5% change in BFP expression **(Figure S4D)**. This level of collateral damage had no detectable effects on cell viability **(Figure S2G),** let alone the fact that it was induced by an overwhelmingly abundant GFP target, which might never occur for native targets. These results indicated that the MONARCH 2.0 system effectively improved overall on-target activity characteristics while still preserving minimal collateral damage.

To assess the safety and effectiveness of MONARCH 2.0 in a close-to-real scenario, we again assessed the dose-dependent downregulation of RNA from a stably integrated gene with MONARCH 2.0, as well as the level of collateral damage potentially introduced to non-target genes with a stably integrated all-in-one testing platform for the MONARCH 2.0 system **(Figure 5E and Figure S4E)**. We observed an improved dynamic range of mCherry expression with Dox induction, indicating a moderately restored level of Cas13d and crRNA at higher dosages **(Figures 5F and Figure S4F)**, and consistently low-noise throughout **(Figures 5G and Figure S4G)**. Compared to MONARCH 1.0, basal target downregulation was further reduced to non-detectable levels when targeting a genomic target. We hypothesized that moderately restored mRNA stability provided more TetR protein and thus resulted in stronger transcriptional repression of crRNA expression, especially without induction **(Figure 5A)**. The maximum on-target reduction reached up to 70% from the basal, much closer to mNF-Cas13d's capability (70% vs. 80%) **(Figures 5H and Figure S4H)**. Similarly, GFP-target expression variation remained stably low, suggesting homogeneous RNA degradation across the cell population **(Figure 5I)**. More importantly, there was no detectable collateral damage to the non-target BFP reporter, suggesting that MONARCH 2.0 remains safe for most target downregulation purposes **(Figure S4I)**.

Finally, we tested how the action of MONARCH 2.0 on the same endogenous gene target BACH1, compared to MONARCH 1.0. By transiently transfecting the same amount of BACH1 crRNA array into MONARCH 2.0 cells **(Figure 5J)**, there was no basal target reduction from uninduced MONARCH 2.0, while tunability of BACH1 mRNA reduction improved up to 70% from the basal **(Figure 4K)**, consistent with observations from synthetic reporter targeting. This demonstrates consistent improvements of the MONARCH 2.0 system over MONARCH 1.0, useful for achieving more effective and precise target RNA downregulation.

Overall, we introduced a further optimization strategy to improve over the on-target activity of MONARCH 1.0 system by incorporating an RNA stabilizing element, Triplex, into the circuit design, generating the upgraded MONARCH 2.0 system. We demonstrated that MONARCH 2.0 effectively improved maximal target reduction while preserving minimal collateral damage,

indicating an even greater potential for broad applications in genetic studies and therapeutic developments.

MONARCH system established in engineered Vero E6 cells demonstrates potential for inducible anti-viral activity

Cas13d, an RNA-guided RNA-targeting nuclease without protospacer flanking sequence (PFS) constraints[36], has demonstrated significant potential as an artificial antiviral effector[37]. However, both our research and other studies have identified that unregulated overexpression of Cas13d and crRNAs can cause substantial collateral damage, severely compromising its utility in therapeutic applications and biological research. Therefore, appropriate regulation of Cas13d is crucial for its safe deployment in any intended application. Here, we illustrate the potential of the MONARCH system as a regulatable antiviral defense mechanism against the COVID-19 virus at the cellular level.

While direct experimentation with the full SARS-CoV-2 virus is challenging, we explored the potential of targeting viral genomic fragments using the MONARCH system engineered into Vero E6 cells, a standard model for human viral studies in Biosafety Level III laboratories. We first assessed the feasibility of employing the same integration techniques used in human cells for generating a landing pad platform at the AAVS1 site of Vero E6 cells. Intriguingly, BLAST alignment revealed a corresponding AAVS1 ortholog in the African Green Monkey (Chlorocebus aethiops) genome, from which the Vero E6 cell line is derived, with a preserved PAM site for the sgRNA used in human cells, albeit with two distant mismatches **(Figure S5A)**. This alignment suggested the potential use of the same LP generation pipeline and sgRNA sequences for LP insertion into the AAVS1 ortholog in Vero E6 cells.

We proceeded to integrate the LP cassette into the Vero E6 genome specifically at the AAVS1 ortholog site by co-transfecting Vero E6 cells with a landing pad donor vector and a helper vector expressing enhanced SpCas9 (eSpCas9) and sgRNA **(Figure S5B)**. To circumvent antibiotic selection conflicts, we replaced the neomycin resistance gene (NeoR), which was previously introduced along with the TMPRSS2 gene into the Vero E6 model cell line we possessed, with a puromycin resistance gene (PuroR) in the LP cassette. We cloned an RFP reporter into the LP donor vector backbone to negatively select against random integration. Following puromycin selection, we successfully isolated a group of surviving Vero cells, all expressing only green fluorescence, from which we established single-cell derived clonal populations **(Figure S5C)**. High and stable GFP expression in these clones suggested that the AAVS1 ortholog might also serve as a safe harbor site in the Vero genome. Subsequently, we employed the same RMCE strategy to site-specifically integrate both the MONARCH system co-expressing crRNA arrays targeting SARS-CoV-2 genome fragments, into the AAVS1 ortholog **(Figure 6A and Figure S5D)**.

Additionally, we constructed a single-plasmid reporter system for SARS-CoV-2 genomic fragments, incorporating partial RdRp and N genes from the SARS-CoV-2 genome into the 3'UTR of a CMV-GFP expression cascade **(Figure 6A)**. Following transfection of Vero E6 cells engineered with both the MONARCH system and wildtype cells (before LP insertion) as controls, we observed that mCherry levels increased in a dose-responsive manner in both MONARCH systems, with comparable dynamic ranges of MONARCH 1.0 and 2.0 **(Figure 6B)**. Both circuits had low CV across all dosages, with MONARCH 1.0 being slightly higher overall **(Figure 6C)**. Furthermore, both systems demonstrated the capacity to reduce GFP reporter

levels in a dose-dependent manner, indicative of an inducible reduction of viral fragments within the Vero E6 cells **(Figure 6D)**.

To further enhance the effectiveness of the MONARCH system, we hypothesized that providing additional crRNA arrays could amplify the reduction of viral fragments by introducing extra targeting crRNAs and creating a decoy effect to reduce Cas13d self-degradation. We tested this by co-transfecting the SARS-CoV-2 reporter cascade with either SARS-CoV-2-targeting crRNA arrays, non-targeting crRNA, or a blank control into 10 ng/ ml pre-induced MONARCH integrated Vero cells. The results confirmed our hypothesis, as even non-targeting crRNA induced more Cas13d expression due to the decoy effect, compared to the blank control, and additional crRNAs as an array resulted in stronger Cas13d induction **(Figure 6F)**. Notably, by transiently introducing extra targeting crRNAs into the cells, on-target activity was further elevated by about 50% and 80% for MONARCH 1.0 and 2.0 respectively, resulting in over 75% and 90% total reduction of viral fragments **(Figure 6G)**.

Overall, these findings suggested that the MONARCH system could be effectively leveraged as a regulatable antiviral defense mechanism at the cellular level. Additionally, the engineered Vero E6 cell model developed in this study could potentially support broader viral studies with a reliable and repeatable genomic integration site, enabling precise, mutation-free, single-copy, site-specific DNA payload insertion and versatile repurposing.

DISCUSSION

The discovery of Cas13d has sparked considerable interest due to its unique RNA-targeting capabilities, which hold immense potential for biotechnological and clinical applications. However, its deployment has been hindered by the occurrence of collateral damage, where nonspecific RNA degradation can occur, leading to significant cell viability issues and global transcriptomic alterations[33] **(Figure S2G)**. Notably, the extent of collateral damage appears closely linked to target abundance, with pronounced effects when targeting highly overexpressed repetitive elements, whereas minimal impact is observed with low-expression genes[33] **(Figures 3C-D and Figure S2C-D)**. This variability may explain the disparate findings across studies regarding Cas13d's collateral damage in mammalian cells, with some research reporting negligible effects[38-40], while others observe significant *trans* cleavage activity[19,33,41]. Despite these challenges, the potential utility of Cas13d in RNA downregulation and as a modular, programmable alternative to traditional RNA interference technologies should not be overlooked. Intriguingly, some studies propose harnessing Cas13d's collateral activity for therapeutic strategies, such as inducing cancer-specific apoptosis through global RNA depletion[42,43]. Therefore, it is crucial for researchers to assess the extent of *trans* cleavage (collateral damage) when employing Cas13d to ensure accurate interpretations of biological effects in their experimental contexts.

Using the precise gene expression-tuning mNF gene circuit to define how target RNA reduction depends on Cas13d and crRNA levels, we found that the expression levels of both Cas13d and crRNA are critical in modulating collateral damage, which seems to behave like a typical enzyme-catalyzed biochemical reaction, dependent on the biochemical context, substrate concentration, enzyme levels, and target binding affinity. Interestingly, our research revealed that the Cas13d:crRNA complex exhibits significant enzymatic activity on its substrate, marked by a unique crRNA binding site, even with minimal amounts of the complex **(Figure 4H and Figure S3C)**. Furthermore, we observed a consistent positive correlation between on-target activity and collateral damage when Cas13d and crRNA were co-expressed at high levels **(Figure 3C-D, G-H and Figure S2C-D)**. Given that *trans* cleavage is an inherent characteristic of Cas13d, we propose that *trans* cleavage may play a critical role in on-target degradation, with a substantial amount of target RNAs are degraded through *trans* cleavage (collateral damage) rather than *cis* cleavage. This also corroborates the observation that the relative abundance of target RNA and activated Cas13d:crRNA complex is a key factor to minimize unwanted collateral damage.

To address the issue of collateral inhibition while maintaining specific RNA downregulation, we developed the MONARCH 1.0 system—a multi-level negative-autoregulation circuit designed to finely tune the expression of Cas13d and crRNA **(Figure 4A)**. Although effective at reducing both collateral damage and basal target reduction, the system lowered too much Cas13d and crRNA expression even at full induction, which inadvertently diminished maximal on-target activity **(Supplementary Figures 3H-I)**. Seeking to balance expression levels without compromising regulatory control, we explored the use of a Triplex motif derived from the mouse non-coding RNA Malat1[34]. We adapted this motif, previously shown to integrate CRISPR-Cas12a with crRNA and maintain robust DNA-targeting activity[35], to potentially restore optimal

Cas13d levels while keeping crRNA expression moderated. This adjustment led to the development of MONARCH 2.0 **(Figure 5A)**, which significantly enhanced the tunability of on-target activity without reintroducing notable collateral damage **(Figure 5H; Figure S4D)**.

An additional surprising outcome from this study was the successful application of our landing-pad-based integration strategy, originally developed for human cells, in Vero E6 cells. The AAVS1 orthologous site in the Vero E6 genome retained functional sgRNA targeting sites and intact homologous regions, enabling precise genomic integration, and opening new opportunities for human virology **(Figure S5A)**. Vero E6 cells engineered with the MONARCH system can robustly target viral genomes **(Figure 6D)**, setting the stage for future realistic viral infection studies and tunable, synthetic antiviral systems. Besides the MONARCH system, we believe that this precisely engineered Vero E6 landing-pad model can hold promise to enable many more viral studies, providing a standard, feasible and robust approach to rapidly generate desired models as desired.

In conclusion, the optimized MONARCH 2.0 circuit we developed precisely controls the expression of Cas13d and crRNA, enabling effective RNA downregulation with minimal collateral damage. By establishing this system in engineered Vero E6 cells, we have illustrated its potential to significantly impact biological research and therapeutic development, particularly in the context of viral infections.

METHODS

Cell culture

HEK293 cells were originally obtained from American Type Culture Collection (ATCC®). All engineered versions of HEK293 cells were cultured in DMEM media with 10% fetal bovine serum (FBS) and 1% penicillin-streptomycin. Vero E6/TMPRSS2 cell line was a gift from Dr. Charles M. Rice at Rockefeller University. All engineered versions of Vero E6 cells were cultured in DMEM media with 10% fetal bovine serum (FBS) and 1% penicillin-streptomycin. Both cell lines were maintained regularly at a 2-4 days interval for each passage based on usage demands. All cell lines and their variants were maintained in Panasonic MCO-170AICUVL-PA cellIQ Series CO_2 Incubators at 37□C and 5% CO_2. The cells were used in experiments within 15 passages after their arrival in the laboratory.

Plasmid Construction

For the generation of the LPutopia-bearing Vero E6 cell line (Vero E6 LP cell), the **LPutopia-8** genome-targeting vector was constructed based on the earlier version LPutopia-7 (Addgene #199212) assembled in the previous studies[28]. Briefly, new selection marker puromycin resistance gene (PuroR) was incorporated into eGFP expression cascade using T2A separation, while original neomycin resistance gene (NeoR) was deleted from the cassette. Every other element was remained the same as LPutopia-7.

For constructing the RMCE vectors, we first built **pUt-mNF-Cas13d** circuit plasmid by replacing the GFP reporter with mCherry-P2A-RfxCas13d target cascade, obtained from pSLQ5428_pHR_EF1a-mCherry-P2A-Rfx_Cas13d-2xNLS-3xFLAG (Addgene #155305), in the previous cloned pUt-mNF-GFP RMCE plasmid[28] (Addgene #199220). Then **MONARCH 1.0** circuit was established by inserting pre-crRNA motif (with GFP-targeting crRNA) right after coding sequences in the 3'UTR region of pUt-mNF-Cas13d plasmid. Further **MONARCH 2.0** circuit was cloned by adding Triplex motif, cloned from pCE048-SiT-Cas12a (Addgene #128124), between coding sequences and pre-crRNA motif. All the all-in-one testing constructs were similarly cloned by inserting SV40-GFP and/or SV40-BFP and/or hU6-2O-crRNA expression cascades into the FRT3/FRT flanking region, to be integrated together with gene circuits via FLP-RMCE simultaneously.

For crRNA plasmids generated in this study, we took the template from pSLQ5429_pUC_hU6-crScaffold_EF1α-BFPv3 (Addgene #155306) and cloned in individual crRNAs using restriction-ligation method. A SV40 replacing EF1α version of BFP-targeting and GFP-targeting crRNA were also cloned. TetR-regulatable hU6 promoter, hU6-2O, was DNA synthesized by IDT with reference sequences taken from previous study[31], then cloned into BFP- and GFP-targeting crRNA plasmids to replace the original hU6 promoter. While BACH1-targeting crRNA array was combined together while individual hU6 promoter was preserved, SARS-CoV-2-targeting crRNA array was assembled into one expression cascade using golden gate assembly. **MONARCH** system was cloned by assembling pre-crRNA or pre-crRNA array from crRNA plasmids with **pUt-mNF-Cas13d** using NEBuilder® HiFi DNA Assembly.

For constructing SARS-CoV-2 genomic fragment targeting reporter plasmid, we first obtained the CoV-2 genomic fragment from pSLQ5080_pHR_PGK_sfGFP_CoV-F2 (Addgene #155304)

and then merged it into the 3'UTR of eGFP expression cascade in LPutopia-7 (Addgene #199212) plasmid, with RFP deleted from the backbone.

The AAVS1-targeting eSpCas9 vector (Addgene #199213) was constructed in the previous study[28]. the codon-optimized FLP recombinase expressing vector-**pCAG-Flpo** also available as Addgene plasmid 60662 was a gift from Dr. Massimo Scanziani. The crRNA template plasmid, SARS-CoV-2-targeting crRNA and non-targeting plasmids, RfxCas13d plasmid and SARS-CoV-2 genomic fragment plasmid were gifts from Dr. Stanley Qi. We used NEBuilder® HiFi DNA Assembly for most of the plasmid cloning. sgRNA and all crRNA sequences used in this study are available in **Supplemental Table 1**.

Transfection and Nucleofection

Lipofection was applied for all HEK293-derived cells. Prior to transfection, cells were plated in 6-well plates and grown to ~80% confluence. Then pCAG-Flpo helper vector and NF-circuit or MONARCH donor vectors were co-transfected at a 1-to-1 ratio with a final mass of 2.5 µg per well. The vectors were first incubated with 3.75 µl of Lipofectamine 3000 (Invitrogen, L3000-015) in OPTI-MEM media (Gibco, 31985062) for 15-30 minutes. The resulting DNA-lipid complex was then pipetted onto the cell culture. Cells were then incubated for at least 24 hours before refreshing media. Appropriate drugs for selection were added 72 hours post-transfection. Drug selection lasted for at least 14 days before FACS cell sorting. We used 10 µg/ml Blasticidin with 10 µg/ml ganciclovir for all the HEK293 engineering cell selection.

For all Vero E6 and its derived cells, Nucleofection was performed based on the manufacturer's instructions and recommendations. Briefly, newly thawed Vero E6 cells were plated in a T-25 flask and sub-cultured 3-5 days before Nucleofection. Next, cells were harvested by adding trypsin and counted using a Cellometer Auto T4 (Nexcelom Bioscience). Around $1x10^6$ cells were collected and centrifuged at 200 x g for 10 minutes at room temperature. Then the supernatant was removed and cells were resuspended in 100 µl room-temperature Nucleofector® Kit V (Lonza, VCA-1003) solution. The LPutopia-8/espCas9 or pCAG-Flpo/MONARCH donor vector combinations were co-transfected at a 1-to-1 ratio with a final mass of 2 µg per sample. The cell/DNA suspension was transferred into the certified Nucleofector® cuvette and the V-001 program of Nucleofector® 2b Device (Lonza, AAB-1001) was applied. Finally, transfected cells were buffered with fresh media and gently transferred into a freshly prepared 6-well plate. Drug Selection started 24-48 hours post-nucleofection and lasted for at least 14 days before FACS cell sorting. We used 4 µg/ml of puromycin for Vero E6 LP cell selection and 2 µg/ml Blasticidin with 5 µg/ml ganciclovir for Vero E6 MONARCH cell selection.

For all the transient transfection assays, engineered HEK293 cells were seeded and induced 72 hours prior to plasmid transfection using Lipofectamine 3000 as described above, while engineered Vero E6 cells were collected after 72-hour pre-induction for nucleofection with plasmids then plated back into 6-well plates for incubation. For both cases, corresponding Dox induction levels were maintained during plasmid incubation, and 72 hours incubation was typically applied prior to flow cytometry or cell viability assay.

Flow cytometry

For each sample, cells were cultured for one passage prior to experimentation. Subsequently, approximately 50,000 to 80,000 cells, harvested from T-25 flasks at 80% confluence, were seeded into 24-well plates, maintaining three technical replicates for each concentration of the

inducer. Doxycycline (Dox) was added to each well to achieve concentrations ranging from 0.01 to 100 ng/ml. The cells were then incubated for 72 hours before being transferred to a 96-well plate, with a final volume of 250 µl per well. Flow cytometry analysis was conducted using a BD LSRFortessa™ flow cytometer equipped with a High Throughput Sampler (HTS) at the Stony Brook Genomics Core Facility. We collected multiple fluorescence signal data for each Dox concentration, recording at least 10,000 events for stably integrated targets and 50,000 for transiently provided targets within a predefined FSA/SSA gate. GFP intensity was measured using the FITC channel, mCherry intensity via the Texas-Red channel, and BFP intensity from the Pacific-Blue channel, maintaining identical PMT voltage settings across all samples and induction levels.

RNA isolation and RT-qPCR

For BACH1 downregulation RT-qPCR test, 100-300k HEK cells were first pre-induced for 72 hours with each Dox concentration in 6-well plates prior to BACH1-targeting crRNA transfection. 144 hours (6-day) after transfection, RNA was then isolated using the RNeasy Plus Mini Kit (Qiagen, 74134). 1 µg of total RNA from each sample was converted to cDNA using iScript™ Reverse Transcription Supermix (Bio-Rad, 1708841). Then qPCR reactions were set up using TaqMan® Fast Advanced Master Mix (ThermoFisher Scientific, 4444557) with TaqMan® Gene Expression Assay and run using the QuantStudio™ 3 Real-Time PCR System (Eppendorf, A28137) at standard curve mode, using the BACH1 TaqMan® probe () and GAPDH reference probe () in a multiplexing setup. Eventually, BACH1 mRNA level quantitation was calculated with reference to the GAPDH level in three independent repeats.

Cell viability assay

For cell viability assays, cells were Dox-induced 72 hours before seeding and 3,000 – 5,000 cells of each induction condition were plated in 96-well plates with 4 replicates with Dox level maintained. Around 6 hours after seeding, transfection of corresponding plasmid or plasmid combinations were applied into settled cells in 96-well plates. all the seeded wells were assayed using alamarBlue™ HS Cell Viability Reagent (Invitrogen, A50100) for viable cells 72 hours post-transfection with dox level maintained throughout. To measure multi-day proliferation, total 6 replicates were seeded at the beginning and then 3 replicates were assessed every 24 hours.
Cells were incubated in alamarBlue reagent for 4 hours and then taken for absorbance measurement at wavelengths of 570 nm and 600 nm with media blank control using Tecan Infinite Pro 200 (Tecan U.S. INC) spectrophotometer. Each absorbance value was adjusted by subtracting the media blank absorbance at the same wavelength. Cell proliferation was measured as the alamarBlue reduction score (S) calculated as:

$$S = (O_2 \times A_{570}) - (O_1 \times A_{600})$$

Where O_1 and O_2 are the molar extinction coefficients of oxidized alamarBlue at 570 nm and 600 nm, respectively; and A_{570} and A_{600} are the absorbances of test wells at 570 nm and 600 nm, respectively. Relative cell viability was then calculated as the relative differences between the average scores of the treated wells to untreated control wells.

Data processing and statistical analysis

Flow cytometry data were analyzed with the FlowJo® software version 10 (Becton, Dickinson and Company). Forward-scatter and side-scatter gates were predefined for each cell type or assay based on the reference sample pretests to exclude debris. Also, a fluorescence-based gate was imposed for FACS cell sorting for desired target cells. Most of the data plots as well as statistical analysis were generated and performed using GraphPad Prism 8 (GraphPad

Software). Statistical details are in the figure legends, including the statistical tests used. In all figures, results were presented as means ± S.D. unless otherwise noted in the figure legend. *$P < 0.05$ was considered statistically significant, indicated by "*" in the figure legend.

FIGURE LEGENDS

Figure 1. Integration of the mNF-Cas13d gene circuit by using a landing-pad platform and recombinase-mediated cassette exchange.

(A) Diagram of engineered HEK 293 cell with a single-copy landing pad located in the AAVS1 safe harbor site. FRT, FRT3: Flp-recombinase target sites; NeoR: Neomycin Resistance Gene; HSV-TK: Herpes Simplex Virus (HSV) thymidine kinase (TK); eGFP: enhanced Green Fluorescence Protein.

(B) Left panel: Schematic diagram of repeatable AAVS1 site-specific integration of genetic payloads such as mNF-Cas13d gene circuit through Flp-recombinase-mediated cassette exchange (FLP-RMCE). **Right panel:** RMCE-based integration will result in a DNA construct switching between donor plasmid and target site. Successful integration of mNF-Cas13d gene circuit shifted the fluorescence signal from green (eGFP) to red (mCherry). HSV-TK in the donor plasmid backbone serves as a negative selection marker against random integration.

(C) Diagram of synthetic mNF gene circuit for Dox-controlled tuning of co-expressed tetracycline repressor (TetR), mCherry reporter and Cas13d protein levels after site-specific integration. TetO: Tetracycline Operator; P2A: self-cleaving peptide.

(D) Representative dose-responses of fluorescence intensity histograms from stably integrated mNF-Cas13d gene circuit measured at 0, 0.01, 0.02, 0.05, 0.1, 0.2, 0.5, 1, 2, 5, 10, 100 ng/ml Dox levels, respectively.

(E) Dose-responses of mean fluorescence intensity of mCherry reporter for stably integrated mNF-Cas13d gene circuit in HEK 293 cells (n=3).

(F) Dose-responses of coefficient of variation (CV) of mCherry reporter for stably integrated mNF-Cas13d gene circuit in HEK 293 cells (n=3).

Figure 2. Negative autoregulation of both Cas13d protein and crRNA improves dose-response characteristics.

(A) Diagram of single-vector transfection to test Cas13d dose-dependent on-target activity. Plasmid encoding BFP reporter and BFP targeting guide or non-targeting guide were transfected into mNF-Cas13d stably integrated HEK 293 cells with corresponding doxycycline (Dox) induction and incubated for 72 hours before flow cytometry.

(B) Dose-responses of mean fluorescence intensity of mCherry reporter for stably integrated mNF-Cas13d gene circuit in HEK 293 cells 72 hours post-transfection. unpaired two-tailed t-test, n=3, **P<0.01, ***P<0.001.

(C) Dose-dependent reduction of transiently transfected BFP reporter induced by Cas13d targeting. All the BFP expression levels were normalized to uninduced sample with non-targeting guide, n = 3.

(D) Diagram of single-vector transfection to test Cas13d dose-dependent on-target activity with regulated crRNA expression. crRNA targeting BFP was expressed from a synthetically modified human U6 (hU6) promoter containing two Tetracycline Operator (TetO2) sites flanking the TATA-box. hU6-2O promoter can be then repressed by Tetracycline Repressor (TetR) expressed from mNF-Cas13d gene circuit.

(E) Comparison of mCherry dose-responses from the mNF-Cas13d gene circuit 72 hours post-transfection with all three transfection constructs. unpaired two-tailed t-test, n=3, **P<0.01, ***P<0.001.

(F) Comparison of dose-dependent BFP reduction induced by Cas13d targeting 72 hours post-transfection with all three transfection constructs. All the BFP expression levels were normalized to uninduced sample with non-targeting guide, n = 3.

(G) Diagram of all-in-one constructs to test Cas13d on-target activity by stably expressing targets from the genome. crRNA targeting the GFP reporter is expressed from the TetR-regulated hU6 promoter while the non-targeting guide is freely expressed from the regular hU6 promoter. The whole construct is integrated via FLP-RMCE using the same HEK 293 Landing pad parental cells.

(H) Dose-responses of mean fluorescence intensity of mCherry reporter for stably integrated all-in-one constructs in HEK 293 cells 72 hours post-induction. unpaired two-tailed t-test, n=3, **P<0.01, ***P<0.001.

(I) Dose-dependent reduction of stably integrated GFP reporter by Cas13d targeting. All GFP expression levels were normalized to uninduced sample with non-targeting guide, n = 3.

Figure 3. Collateral damage induced by activation of Cas13d is dependent on Cas13d and crRNA expression levels.

(A) Diagram of experimental setup to assess collateral damage from activated Cas13d with different guide expression regulation. Target GFP expressed from SV40 promoter was co-transfected with either TetR-regulated GFP-targeting crRNA, constitutively expressing GFP-targeting crRNA or non-targeting crRNA. All three crRNA plasmids contain the same BFP gene expressed from EF1α promoter. Cells were transfected while induced 72 hours before flow cytometry.

(B) Comparison of mCherry dose-responses from the mNF-Cas13d gene circuit 72 hours post-transfection with all three co-transfection setups. unpaired two-tailed t-test, n=3, **P<0.01.

(C) Comparison of relative GFP levels indicating on-target activity dose-responses from the mNF-Cas13d gene circuit 72 hours post-transfection with all three co-transfection setups. All the GFP expression levels were normalized to uninduced sample with non-targeting guide, n=3.

(D) Comparison of relative BFP levels indicating off-target activity dose-responses from the mNF-Cas13d gene circuit 72 hours post-transfection with all three co-transfection setups. All the BFP expression levels were normalized to uninduced sample with non-targeting guide, n=3.

(E) Diagram of all-in-one constructs to test Cas13d on-target activity and off-target activity by stably expressing targets from the genome. crRNA-targeting the GFP reporter is expressed from the TetR-regulated hU6 promoter while the non-targeting guide is freely expressed from normal hU6 promoter. The whole construct is integrated via FLP-RMCE using the same HEK 293 Landing pad parentals.

(F) Dose-responses of mCherry reporter indicating Cas13d expression levels for stably integrated all-in-one constructs in HEK 293 cells 72 hours post-induction. unpaired two-tailed t-test, n=3, *P<0.05, **P<0.01.

(G) Dose-responses of relative GFP reporter levels indicating on-target activity for stably integrated all-in-one constructs in HEK 293 cells 72 hours post-induction. All the GFP expression levels were normalized to uninduced sample with non-targeting guide, n=3.

(H) Dose-responses of relative BFP reporter levels indicating off-target activity for stably integrated all-in-one constructs in HEK 293 cells 72 hours post-induction. All the BFP expression levels were normalized to uninduced sample with non-targeting guide, n=3.

Figure 4. Multi-level negative autoregulation of Cas13d and crRNA reduces the basal target downregulation.

(A) Design and rationale for multi-level negative-autoregulation for Cas13d and crRNA expression. Overexpression of both Cas13d and crRNA likely produce many activated Cas13d:crRNA complexes causing strong basal target reduction and collateral damage. Incorporating the crRNA into the same transcript with Cas13d not only brings both under the same tight transcriptional regulation but also adds a layer of RNA-level regulation via crRNA processing by Cas13d itself. This may greatly reduce the basal target reduction as well as the collateral damage.

(B) Representative dose-responses of fluorescence intensity histograms from stably integrated MONARCH 1.0 circuit measured at 0, 0.1, 0.2, 0.5, 1, 10 ng/ml Dox levels, respectively.

(C) Dose-responses of mean fluorescence intensity of mCherry reporter for stably integrated MONARCH 1.0 circuit in HEK 293 cells (n=3).

(D) Dose-responses of coefficient of variation (CV) of mCherry reporter for stably integrated MONARCH 1.0 in HEK 293 cells (n=3).

(E) Diagram to test on-target activity of Cas13d expressed from MONARCH 1.0 by stably expressing targets from the genome. The whole construct is integrated via FLP-RMCE using the same HEK 293 Landing pad parentals. Basal level is determined with integration of only GFP target expressed from the SV40 promoter.

(F) Dose-responses of mean fluorescence intensity of mCherry reporter for stably integrated MONARCH 1.0_SV40-GFP construct in HEK 293 cells (n=3).

(G) Dose-responses of coefficient of variation (CV) of mCherry reporter for stably integrated MONARCH 1.0_SV40-GFP in HEK 293 cells (n=3).

(H) Dose-responses of relative GFP levels indicating on-target activity for stably integrated MONARCH 1.0_SV40-GFP construct in HEK 293 cells. All the GFP expression levels were normalized to the basal sample, n=3.

(I) Dose-responses of coefficient of variation (CV) of target GFP reporter for stably integrated MONARCH 1.0_SV40-GFP in HEK 293 cells (n=3).

(J) Diagram to test on-target activity of MONARCH 1.0 on the endogenous target other than the carrying crRNA. crRNA-targeting GFP serves only as a RNA-level regulator in this scenario. Multiple crRNAs targeting BACH1 are cloned into a single plasmid and transfected together. RT-qPCR was performed after 144 hours induction and incubation post-transfection.

(K) Dose-dependent reduction of endogenous BACH1 induced by Cas13d targeting for stably integrated MONARCH 1.0 in HEK 293 cells. One-way ANOVA with Tukey's multiple comparisons tests between each dose and native control, n=3.

Figure 5. Optimized multi-level negative autoregulation of Cas13d and crRNA improves on-target cutting and minimizes basal target reduction.

(A) Design and rationale for optimized multi-level negative-autoregulation for Cas13d and crRNA expression. Compared to the MONARCH 1.0, a tertiary RNA structural motif “Triplex” is incorporated between CDS and crRNA in order to stabilize transcripts lacking poly(A) due to crRNA processing, enabling moderately extended window of protein expression.

(B) Representative dose-responses of fluorescence intensity histograms from stably integrated MONARCH 2.0 circuit measured at 0, 0.1, 0.2, 0.5, 1, 10 ng/ml Dox levels, respectively.

(C) Dose-responses of mean fluorescence intensity of mCherry reporter for stably integrated MONARCH 2.0 circuit in HEK 293 cells (n=3).

(D) Dose-responses of coefficient of variation (CV) of mCherry reporter for stably integrated MONARCH 2.0 in HEK 293 cells (n=3).

(E) Diagram to test on-target activity of Cas13d expressed from MONARCH 2.0 by stably expressing targets from the genome. The whole construct is integrated via FLP-RMCE using the same HEK 293 Landing pad parentals. Basal level is determined with integration of only GFP target expressed from the SV40 promoter.

(F) Dose-responses of mean fluorescence intensity of mCherry reporter for stably integrated MONARCH 2.0_SV40-GFP construct in HEK 293 cells (n=3).

(G) Dose-responses of coefficient of variation (CV) of mCherry reporter for stably integrated MONARCH 2.0_SV40-GFP in HEK 293 cells (n=3).

(H) Dose-responses of relative GFP levels indicating on-target activity for stably integrated MONARCH 2.0_SV40-GFP construct in HEK 293 cells. All the GFP expression levels were normalized to the basal sample, n=3.

(I) Dose-responses of coefficient of variation (CV) of target GFP reporter for stably integrated MONARCH 2.0_SV40-GFP in HEK 293 cells (n=3).

(J) Diagram to test on-target activity of MONARCH 2.0 on the endogenous target other than the carrying crRNA. crRNA-targeting GFP serves only as a RNA-level regulator in this scenario. Multiple crRNAs targeting BACH1 are cloned into a single plasmid and transfected together. RT-qPCR was performed after 144 hours induction and incubation post-transfection.

(K) Dose-dependent reduction of endogenous BACH1 induced by Cas13d targeting for stably integrated MONARCH 2.0 in HEK 293 cells. One-way ANOVA with Tukey's multiple comparisons tests between each dose and native control, n=3.

Figure 6. MONARCH system established in Vero E6 cells demonstrates tunable anti-viral activity and potential to further improve on-target efficiency.

(A) Diagram of experimental setup to repurpose the MONARCH system to target SARS-CoV-2 genome fragments in engineered Vero cells. Both MONARCH systems were stably integrated into the AAVS1 ortholog in Vero E6 genome using the same Landing-Pad and RMCE strategy. SARS-CoV-2 genome fragments are cloned into the 3'UTR of the GFP transcript, and successful targeting on them by Cas13d will result in mRNA degradation, which can be measured by GFP fluorescence reduction.

(B) Comparison of mCherry dose-responses from MONARCH 1.0 and 2.0 stably integrated in Vero cell 72 hours post-transfection.

(C) Comparison of coefficient of variation (CV) of mCherry dose-responses from MONARCH 1.0 and 2.0 stably integrated in Vero cell 72 hours post-transfection.

(D) Comparison of relative GFP levels indicating on-target activity dose-responses from MONARCH 1.0 and 2.0 stably integrated in Vero cell 72 hours post-transfection. All the GFP expression levels were normalized to native Vero cells transfected with target plasmid only. Unpaired two-tailed t-test for each dosage comparison, n=3, **P<0.01, ***P<0.001.

(E) Diagram of experimental setup to assess further improvement of MONARCH on-target activity by externally providing extra crRNA. Target donor plasmid is co-transfected with either SARS-CoV-2-targeting CRISPR array, non-targeting crRNA or blank control into the engineered Vero cells. Engineered Vero cells are pre-induced with 10 ng/ml doxycycline 72 hours before transfection.

(F) Relative mCherry expression increases from 10 ng/ml doxycycline pre-induced MONARCH 1.0 and 2.0 stably integrated in Vero cell 72 hours post-transfection with extra crRNA plasmids. All the mCherry expression levels were normalized to the Vero cells transfected with Blank control plasmid.

(G) Relative GFP levels reduction 72 hours post-transfection with extra crRNA plasmids. All the GFP expression levels were normalized to the Vero cells transfected with Blank control plasmid.

ACKNOWLEDGMENTS

We thank Dr. S. Lei Qi for sharing the Cas13d-encoding plasmid, the GFP-SARS-CoV-2 fragments (SARS-CoV-2-F1 and SARS-CoV-2-F2) as well as crRNAs targeting these fragments, Dr. Feng Zhang for sharing espCas9, Dr. Massimo Scanziani for sharing the Flp recombinase and Dr. Charles M. Rice for the Vero E6 cell line. We thank Dr. Erich R. Mackow and the Balázsi lab members for insightful discussions and comments. GB was supported by the National Institutes of Health, NIGMS MIRA Program (R35 GM122561), by Stony Brook Cancer Center Engineering, Physical Sciences and Oncology Pilot Funds, by Stony Brook University's Office of the Vice President for Research Seed Grant Program, and by the Laufer Center for Physical and Quantitative Biology.

AUTHOR CONTRIBUTIONS

Conceptualization, Y.W., and G.B.; Formal Analysis, Y.W. and G.B.; Methodology, Y.W.,. and G.B.; Investigation, Y.W., D.C., C.H., and G.B.; Data Curation and Visualization, Y.W. C.H. and G.B.; Writing –Original Draft, Y.W. and G.B.; Writing – Review & Editing, Y.W., and G.B.; Funding Acquisition and Resources, G.B.; Supervision, G.B.; Project Administration, G.B.

DECLARATION OF INTERESTS

The authors declare no conflicts of interest.

DATA AND CODE AVAILABILITY

All materials, code and data will also be available by the lead contact upon request.

Additionally, we will deposit some of the plasmids generated from this study with Addgene.

REFERENCES

1 Jinek, M. *et al.* A programmable dual-RNA-guided DNA endonuclease in adaptive bacterial immunity. *Science* **337**, 816-821, doi:10.1126/science.1225829 (2012).

2 Doudna, J. A. & Charpentier, E. Genome editing. The new frontier of genome engineering with CRISPR-Cas9. *Science* **346**, 1258096, doi:10.1126/science.1258096 (2014).

3 Koonin, E. V., Makarova, K. S. & Zhang, F. Diversity, classification and evolution of CRISPR-Cas systems. *Curr Opin Microbiol* **37**, 67-78, doi:10.1016/j.mib.2017.05.008 (2017).

4 Wright, A. V., Nunez, J. K. & Doudna, J. A. Biology and Applications of CRISPR Systems: Harnessing Nature's Toolbox for Genome Engineering. *Cell* **164**, 29-44, doi:10.1016/j.cell.2015.12.035 (2016).

5 Pickar-Oliver, A. & Gersbach, C. A. The next generation of CRISPR-Cas technologies and applications. *Nat Rev Mol Cell Biol* **20**, 490-507, doi:10.1038/s41580-019-0131-5 (2019).

6 Zhu, H., Li, C. & Gao, C. Applications of CRISPR-Cas in agriculture and plant biotechnology. *Nat Rev Mol Cell Biol* **21**, 661-677, doi:10.1038/s41580-020-00288-9 (2020).

7 Conrad, B. & Antonarakis, S. E. Gene duplication: a drive for phenotypic diversity and cause of human disease. *Annu Rev Genomics Hum Genet* **8**, 17-35, doi:10.1146/annurev.genom.8.021307.110233 (2007).

8 Stefansson, H. *et al.* Large recurrent microdeletions associated with schizophrenia. *Nature* **455**, 232-236, doi:10.1038/nature07229 (2008).

9 Cooper, G. M. *et al.* A copy number variation morbidity map of developmental delay. *Nat Genet* **43**, 838-846, doi:10.1038/ng.909 (2011).

10 Glessner, J. T. *et al.* Increased frequency of de novo copy number variants in congenital heart disease by integrative analysis of single nucleotide polymorphism array and exome sequence data. *Circ Res* **115**, 884-896, doi:10.1161/CIRCRESAHA.115.304458 (2014).

11 Wellcome Trust Case Control, C. *et al.* Genome-wide association study of CNVs in 16,000 cases of eight common diseases and 3,000 shared controls. *Nature* **464**, 713-720, doi:10.1038/nature08979 (2010).

12 Gilbert, L. A. *et al.* Genome-Scale CRISPR-Mediated Control of Gene Repression and Activation. *Cell* **159**, 647-661, doi:10.1016/j.cell.2014.09.029 (2014).

13 Becirovic, E. Maybe you can turn me on: CRISPRa-based strategies for therapeutic applications. *Cell Mol Life Sci* **79**, doi:ARTN 130

10.1007/s00018-022-04175-8 (2022).

14 Larson, M. H. *et al.* CRISPR interference (CRISPRi) for sequence-specific control of gene expression. *Nat Protoc* **8**, 2180-2196, doi:10.1038/nprot.2013.132 (2013).

15 Cui, L. *et al.* A CRISPRi screen in E. coli reveals sequence-specific toxicity of dCas9. *Nat Commun* **9**, 1912, doi:10.1038/s41467-018-04209-5 (2018).

16 Howe, F. S. *et al.* CRISPRi is not strand-specific at all loci and redefines the transcriptional landscape. *Elife* **6**, doi:10.7554/eLife.29878 (2017).

17 Abudayyeh, O. O. *et al.* C2c2 is a single-component programmable RNA-guided RNA-targeting CRISPR effector. *Science* **353**, doi:ARTN aaf5573

10.1126/science.aaf5573 (2016).

18 Shi, P. *et al.* Collateral activity of the CRISPR/RfxCas13d system in human cells. *Commun Biol* **6**, 334, doi:10.1038/s42003-023-04708-2 (2023).

19 Wang, Q. *et al.* The CRISPR-Cas13a Gene-Editing System Induces Collateral Cleavage of RNA in Glioma Cells. *Adv Sci (Weinh)* **6**, 1901299, doi:10.1002/advs.201901299 (2019).

20 Wessels, H. H. *et al.* Prediction of on-target and off-target activity of CRISPR-Cas13d guide RNAs using deep learning. *Nat Biotechnol*, doi:10.1038/s41587-023-01830-8 (2023).
21 Ding, Y., Tous, C., Choi, J., Chen, J. & Wong, W. W. Orthogonal inducible control of Cas13 circuits enables programmable RNA regulation in mammalian cells. *Nat Commun* **15**, 1572, doi:10.1038/s41467-024-45795-x (2024).
22 Nevozhay, D., Adams, R. M., Murphy, K. F., Josic, K. & Balazsi, G. Negative autoregulation linearizes the dose-response and suppresses the heterogeneity of gene expression. *P Natl Acad Sci USA* **106**, 5123-5128, doi:10.1073/pnas.0809901106 (2009).
23 Nevozhay, D., Zal, T. & Balázsi, G. Transferring a synthetic gene circuit from yeast to mammalian cells. *Nat Commun* **4**, 1-11, doi:10.1038/ncomms2471 (2013).
24 Guinn, M. T. & Balazsi, G. Noise-reducing optogenetic negative-feedback gene circuits in human cells. *Nucleic Acids Res* **47**, 7703-7714, doi:10.1093/nar/gkz556 (2019).
25 Szenk, M., Yim, T. & Balazsi, G. Multiplexed Gene Expression Tuning with Orthogonal Synthetic Gene Circuits. *Acs Synth Biol* **9**, 930-939, doi:10.1021/acssynbio.9b00534 (2020).
26 Farquhar, K. S. *et al.* Role of network-mediated stochasticity in mammalian drug resistance. *Nat Commun* **10**, 2766, doi:10.1038/s41467-019-10330-w (2019).
27 Wan, Y. *et al.* Adaptive DNA amplification of synthetic gene circuit opens a way to overcome cancer chemoresistance. *Proc Natl Acad Sci U S A* **120**, e2303114120, doi:10.1073/pnas.2303114120 (2023).
28 Wan, Y. *et al.* Nonmonotone invasion landscape by noise-aware control of metastasis activator levels. *Nat Chem Biol* **19**, 887-899, doi:10.1038/s41589-023-01344-z (2023).
29 Nevozhay, D., Zal, T. & Balazsi, G. Transferring a synthetic gene circuit from yeast to mammalian cells. *Nat Commun* **4**, 1451, doi:10.1038/ncomms2471 (2013).
30 Guinn, M. T. & Balázsi, G. Noise-reducing optogenetic negative-feedback gene circuits in human cells. *Nucleic acids research* **47**, 7703-7714, doi:10.1093/nar/gkz556 (2019).
31 Sun, N. *et al.* Development of drug-inducible CRISPR-Cas9 systems for large-scale functional screening. *BMC Genomics* **20**, 225, doi:10.1186/s12864-019-5601-9 (2019).
32 Tong, H. *et al.* High-fidelity Cas13 variants for targeted RNA degradation with minimal collateral effects. *Nat Biotechnol* **41**, 108-119, doi:10.1038/s41587-022-01419-7 (2023).
33 Kelley, C. P., Haerle, M. C. & Wang, E. T. Negative autoregulation mitigates collateral RNase activity of repeat-targeting CRISPR-Cas13d in mammalian cells. *Cell Rep* **40**, 111226, doi:10.1016/j.celrep.2022.111226 (2022).
34 Wilusz, J. E. *et al.* A triple helix stabilizes the 3' ends of long noncoding RNAs that lack poly(A) tails. *Genes Dev* **26**, 2392-2407, doi:10.1101/gad.204438.112 (2012).
35 Campa, C. C., Weisbach, N. R., Santinha, A. J., Incarnato, D. & Platt, R. J. Multiplexed genome engineering by Cas12a and CRISPR arrays encoded on single transcripts. *Nat Methods* **16**, 887-893, doi:10.1038/s41592-019-0508-6 (2019).
36 Yan, W. X. *et al.* Cas13d Is a Compact RNA-Targeting Type VI CRISPR Effector Positively Modulated by a WYL-Domain-Containing Accessory Protein. *Mol Cell* **70**, 327-339 e325, doi:10.1016/j.molcel.2018.02.028 (2018).
37 Abbott, T. R. *et al.* Development of CRISPR as an Antiviral Strategy to Combat SARS-CoV-2 and Influenza. *Cell* **181**, 865-876 e812, doi:10.1016/j.cell.2020.04.020 (2020).
38 Abudayyeh, O. O. *et al.* RNA targeting with CRISPR-Cas13. *Nature* **550**, 280-284, doi:10.1038/nature24049 (2017).
39 Huynh, N., Depner, N., Larson, R. & King-Jones, K. A versatile toolkit for CRISPR-Cas13-based RNA manipulation in Drosophila. *Genome Biol* **21**, 279, doi:10.1186/s13059-020-02193-y (2020).
40 Konermann, S. *et al.* Transcriptome Engineering with RNA-Targeting Type VI-D CRISPR Effectors. *Cell* **173**, 665-676 e614, doi:10.1016/j.cell.2018.02.033 (2018).

41 Ai, Y. X., Liang, D. M. & Wilusz, J. E. CRISPR/Cas13 effectors have differing extents of off-target effects that limit their utility in eukaryotic cells. *Nucleic Acids Research* **50**, doi:10.1093/nar/gkac159 (2022).
42 Li, C. *et al.* CRISPR-CasRx Targeting LncRNA LINC00341 Inhibits Tumor Cell Growth in vitro and in vivo. *Front Mol Biosci* **8**, 638995, doi:10.3389/fmolb.2021.638995 (2021).
43 Jiang, W. *et al.* Precise and efficient silencing of mutant Kras(G12D) by CRISPR-CasRx controls pancreatic cancer progression. *Theranostics* **10**, 11507-11519, doi:10.7150/thno.46642 (2020).

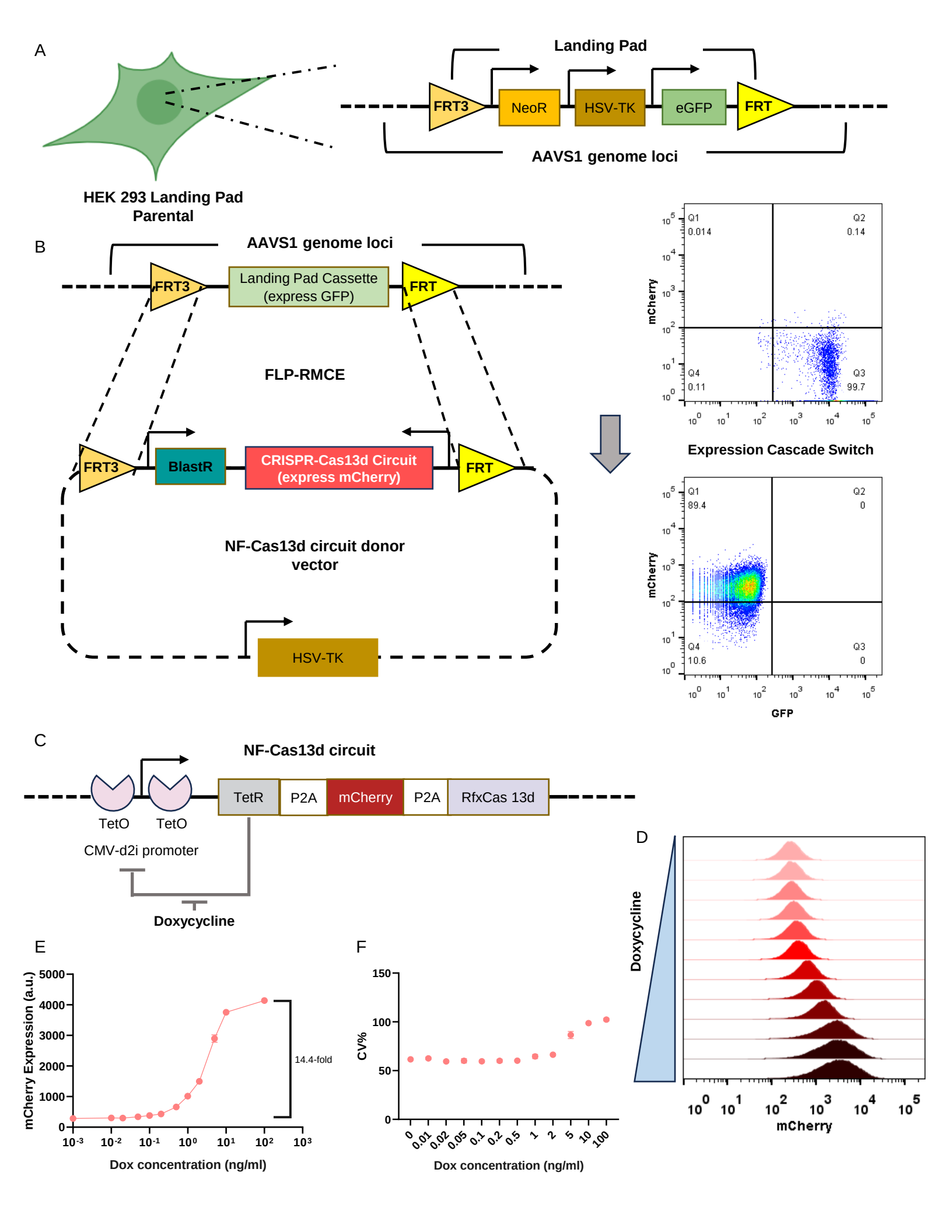
A
Landing Pad
FRT3
NeoR
HSV-TK
eGFP
FRT
AAVS1 genome loci
HEK 293 Landing Pad
Parental
B
AAVS1 genome loci
FRT3
Landing Pad Cassette
(express GFP)
FRT
FLP-RMCE
FRT3
BlastR
CRISPR-Cas13d Circuit
(express mCherry)
FRT
NF-Cas13d circuit donor
vector
HSV-TK
Q1
0.014
Q2
0.14
Q4
0.11
Q3
99.7
mCherry
Expression Cascade Switch
Q1
89.4
Q2
0
Q4
10.6
Q3
0
mCherry
GFP
C
NF-Cas13d circuit
TetO
TetO
CMV-d2i promoter
TetR
P2A
mCherry
P2A
RfxCas 13d
Doxycycline
D
Doxycycline
mCherry
E
mCherry Expression (a.u.)
14.4-fold
Dox concentration (ng/ml)
F
CV%
Dox concentration (ng/ml)

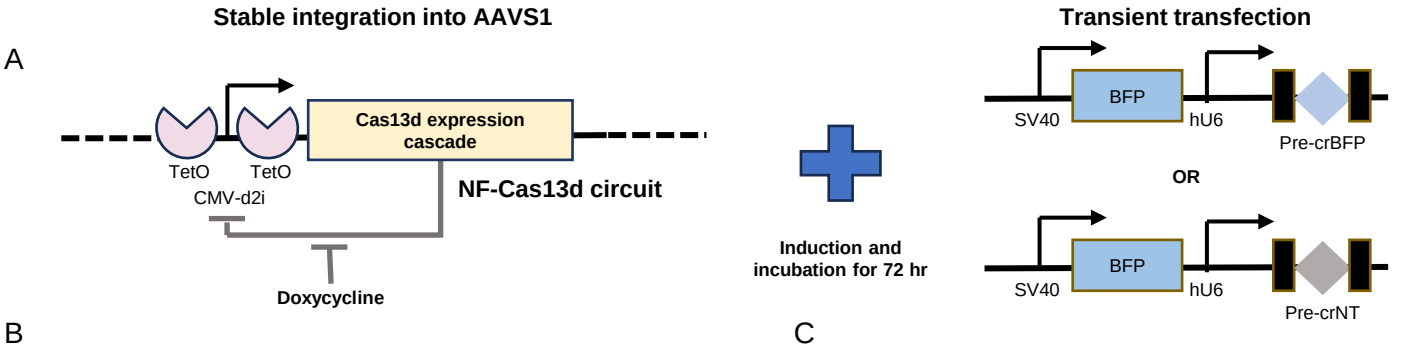
A
Stable integration into AAVS1
Cas13d expression cascade
TetO
TetO
CMV-d2i
NF-Cas13d circuit
Doxycycline
Induction and incubation for 72 hr
Transient transfection
SV40
BFP
hU6
Pre-crBFP
OR
SV40
BFP
hU6
Pre-crNT

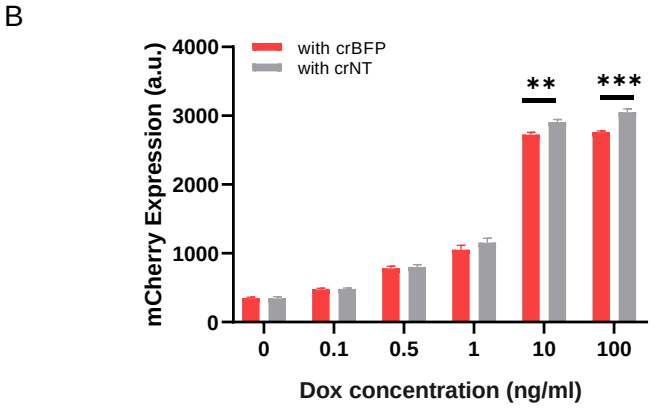
B
with crBFP
with crNT
mCherry Expression (a.u.)
4000
3000
2000
1000
0
**
***
0
0.1
0.5
1
10
100
Dox concentration (ng/ml)

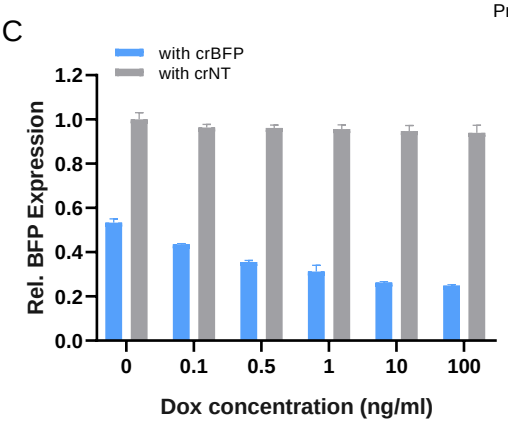
C
with crBFP
with crNT
Rel. BFP Expression
1.2
1.0
0.8
0.6
0.4
0.2
0.0
0
0.1
0.5
1
10
100
Dox concentration (ng/ml)

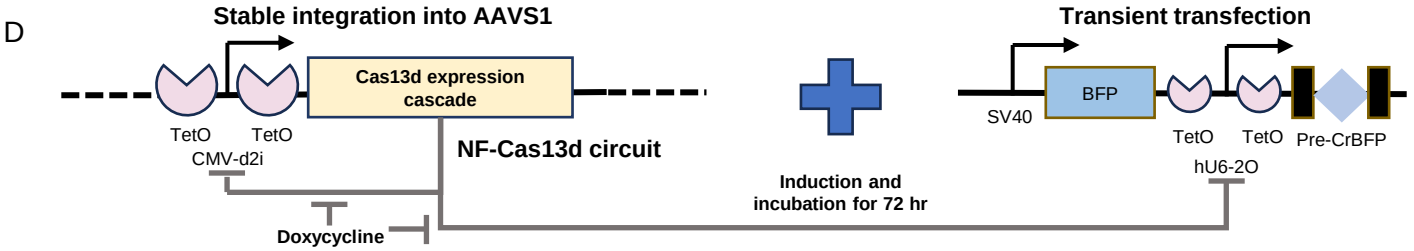
D
Stable integration into AAVS1
Cas13d expression cascade
TetO
TetO
CMV-d2i
NF-Cas13d circuit
Doxycycline
Induction and incubation for 72 hr
Transient transfection
SV40
BFP
TetO
TetO
hU6-2O
Pre-CrBFP

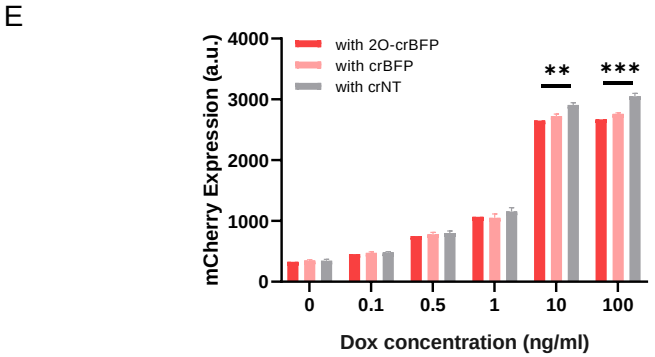
E
with 2O-crBFP
with crBFP
with crNT
mCherry Expression (a.u.)
4000
3000
2000
1000
0
**
***
0
0.1
0.5
1
10
100
Dox concentration (ng/ml)

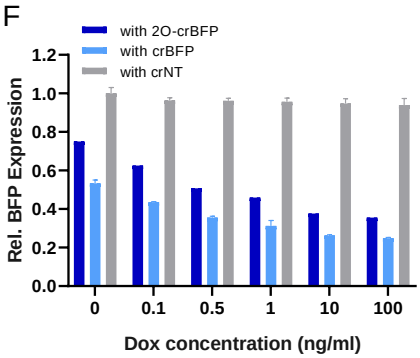
F
with 2O-crBFP
with crBFP
with crNT
Rel. BFP Expression
1.2
1.0
0.8
0.6
0.4
0.2
0.0
0
0.1
0.5
1
10
100
Dox concentration (ng/ml)

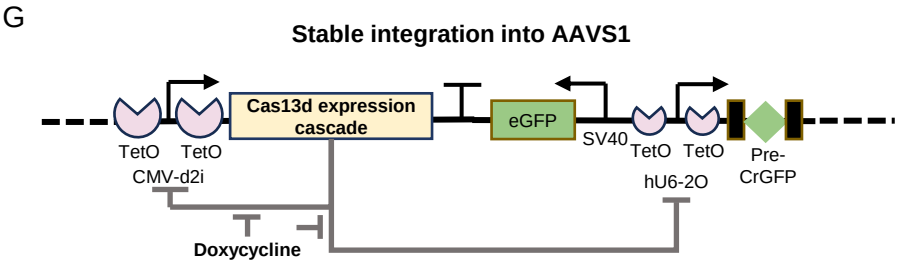
G
Stable integration into AAVS1
Cas13d expression cascade
eGFP
SV40
TetO
TetO
CMV-d2i
TetO
TetO
hU6-2O
Pre-CrGFP
Doxycycline

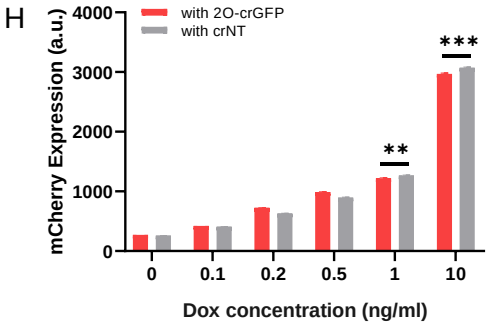
H
with 2O-crGFP
with crNT
mCherry Expression (a.u.)
4000
3000
2000
1000
0
**
***
0
0.1
0.2
0.5
1
10
Dox concentration (ng/ml)

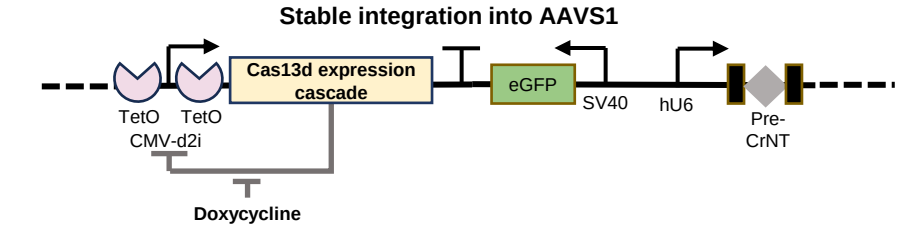
Stable integration into AAVS1
Cas13d expression cascade
eGFP
SV40
hU6
TetO
TetO
CMV-d2i
Pre-CrNT
Doxycycline

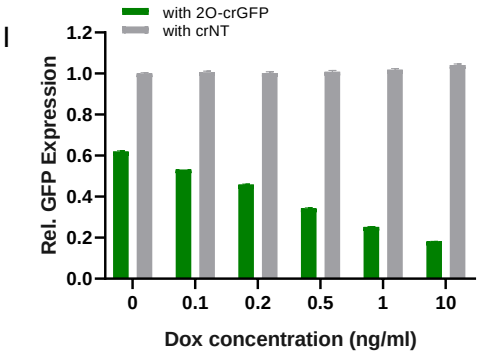
I
with 2O-crGFP
with crNT
Rel. GFP Expression
1.2
1.0
0.8
0.6
0.4
0.2
0.0
0
0.1
0.2
0.5
1
10
Dox concentration (ng/ml)

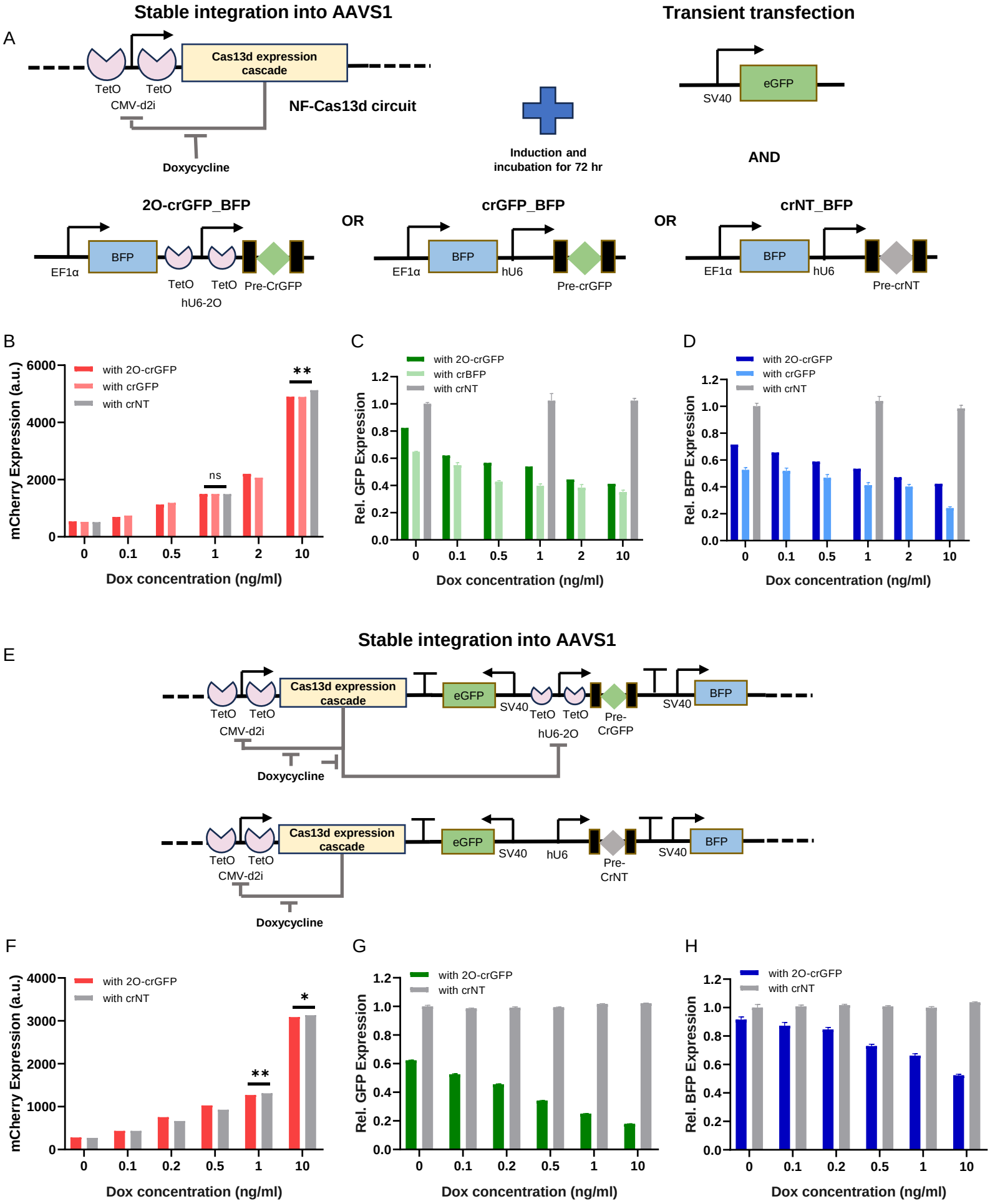
A
Stable integration into AAVS1
Cas13d expression cascade
TetO
TetO
CMV-d2i
NF-Cas13d circuit
Doxycycline
Induction and incubation for 72 hr
Transient transfection
eGFP
SV40
AND
2O-crGFP_BFP
OR
crGFP_BFP
OR
crNT_BFP
BFP
EF1α
TetO
TetO
hU6-2O
Pre-CrGFP
hU6
Pre-crGFP
Pre-crNT
B
mCherry Expression (a.u.)
with 2O-crGFP
with crGFP
with crNT
ns
**
Dox concentration (ng/ml)
C
Rel. GFP Expression
with 2O-crGFP
with crBFP
with crNT
Dox concentration (ng/ml)
D
Rel. BFP Expression
with 2O-crGFP
with crGFP
with crNT
Dox concentration (ng/ml)
E
Stable integration into AAVS1
Cas13d expression cascade
eGFP
SV40
TetO
TetO
hU6-2O
Pre-CrGFP
BFP
CMV-d2i
Doxycycline
hU6
Pre-CrNT
F
mCherry Expression (a.u.)
with 2O-crGFP
with crNT
**
*
Dox concentration (ng/ml)
G
Rel. GFP Expression
with 2O-crGFP
with crNT
Dox concentration (ng/ml)
H
Rel. BFP Expression
with 2O-crGFP
with crNT
Dox concentration (ng/ml)

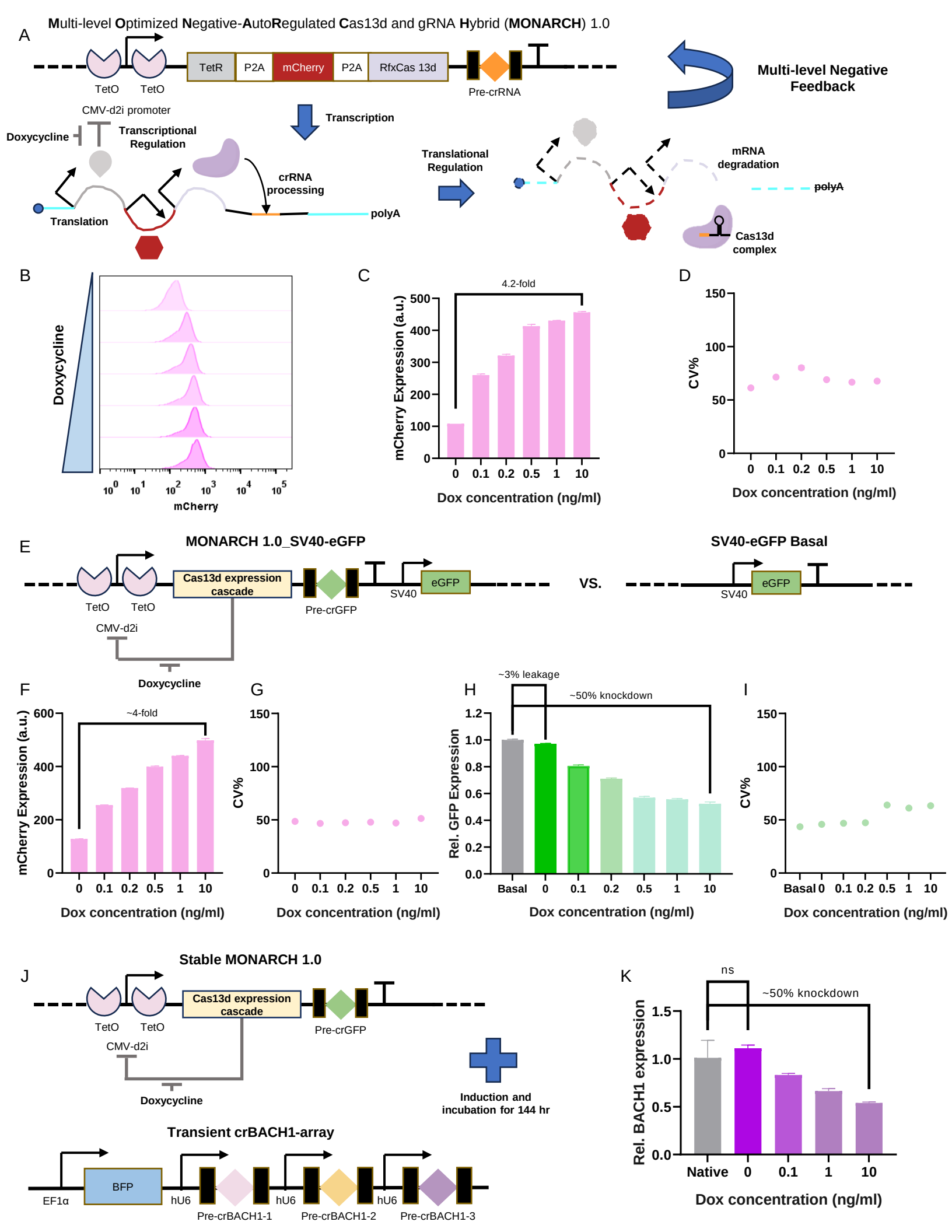
Multi-level Optimized Negative-AutoRegulated Cas13d and gRNA Hybrid (MONARCH) 1.0
A
TetO
TetO
TetR
P2A
mCherry
P2A
RfxCas 13d
Pre-crRNA
Multi-level Negative Feedback
CMV-d2i promoter
Doxycycline
Transcriptional Regulation
Transcription
crRNA processing
Translation
polyA
Translational Regulation
mRNA degradation
polyA
Cas13d complex
B
Doxycycline
mCherry
C
4.2-fold
mCherry Expression (a.u.)
Dox concentration (ng/ml)
D
CV%
Dox concentration (ng/ml)
E
MONARCH 1.0_SV40-eGFP
TetO
TetO
Cas13d expression cascade
Pre-crGFP
SV40
eGFP
CMV-d2i
Doxycycline
VS.
SV40-eGFP Basal
SV40
eGFP
F
~4-fold
mCherry Expression (a.u.)
Dox concentration (ng/ml)
G
CV%
Dox concentration (ng/ml)
H
~3% leakage
~50% knockdown
Rel. GFP Expression
Basal
Dox concentration (ng/ml)
I
CV%
Basal
Dox concentration (ng/ml)
J
Stable MONARCH 1.0
TetO
TetO
Cas13d expression cascade
Pre-crGFP
CMV-d2i
Doxycycline
Induction and incubation for 144 hr
Transient crBACH1-array
EF1α
BFP
hU6
Pre-crBACH1-1
hU6
Pre-crBACH1-2
hU6
Pre-crBACH1-3
K
ns
~50% knockdown
Rel. BACH1 expression
Native
Dox concentration (ng/ml)

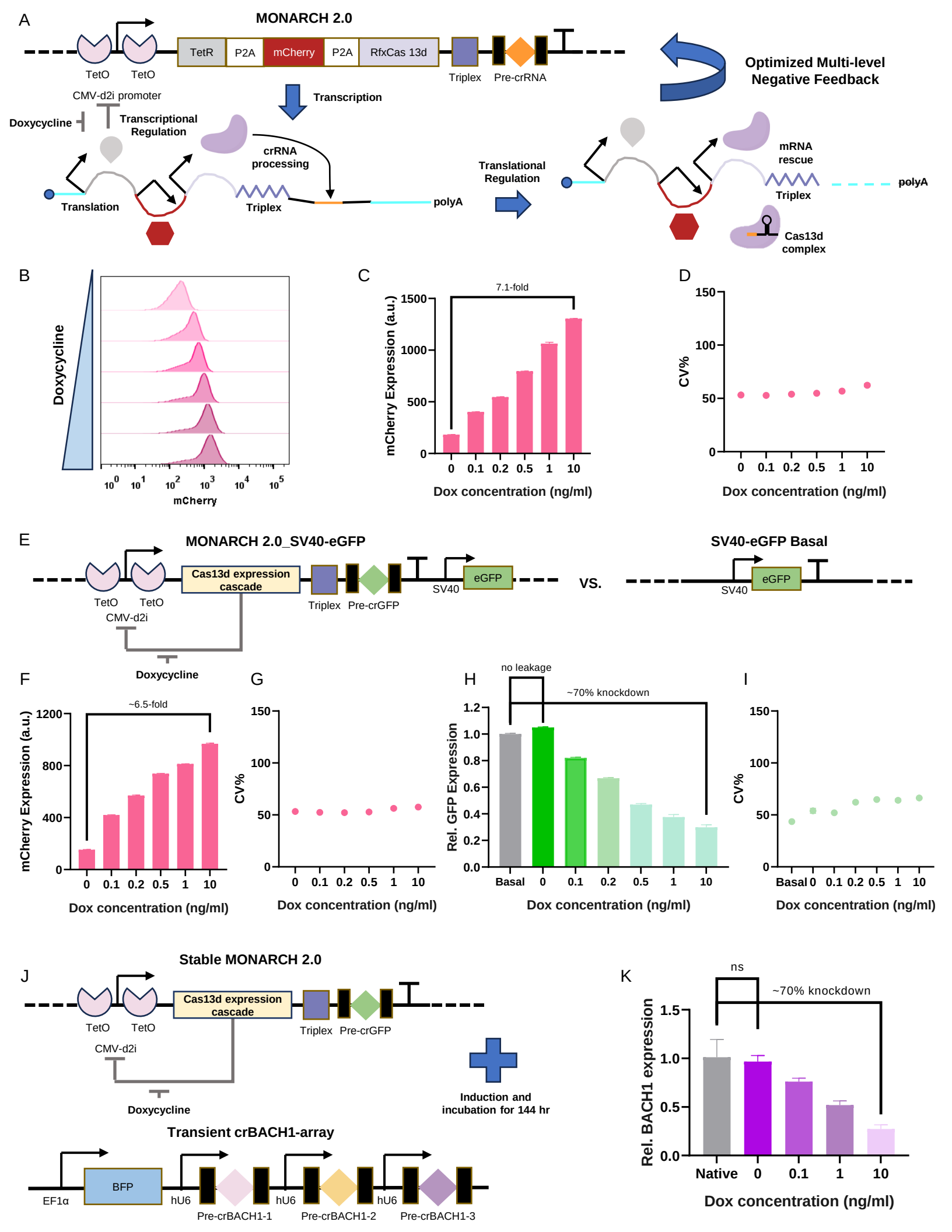
A
MONARCH 2.0
TetR
P2A
mCherry
P2A
RfxCas 13d
TetO
TetO
Triplex
Pre-crRNA
Optimized Multi-level Negative Feedback
CMV-d2i promoter
Transcription
Doxycycline
Transcriptional Regulation
crRNA processing
Translation
Triplex
polyA
Translational Regulation
mRNA rescue
Triplex
polyA
Cas13d complex
B
Doxycycline
mCherry
C
7.1-fold
mCherry Expression (a.u.)
Dox concentration (ng/ml)
D
CV%
Dox concentration (ng/ml)
E
MONARCH 2.0_SV40-eGFP
Cas13d expression cascade
TetO
TetO
CMV-d2i
Triplex
Pre-crGFP
SV40
eGFP
Doxycycline
VS.
SV40-eGFP Basal
SV40
eGFP
F
~6.5-fold
mCherry Expression (a.u.)
Dox concentration (ng/ml)
G
CV%
Dox concentration (ng/ml)
H
no leakage
~70% knockdown
Rel. GFP Expression
Dox concentration (ng/ml)
I
CV%
Dox concentration (ng/ml)
J
Stable MONARCH 2.0
Cas13d expression cascade
TetO
TetO
CMV-d2i
Triplex
Pre-crGFP
Doxycycline
Induction and incubation for 144 hr
Transient crBACH1-array
EF1α
BFP
hU6
hU6
hU6
Pre-crBACH1-1
Pre-crBACH1-2
Pre-crBACH1-3
K
ns
~70% knockdown
Rel. BACH1 expression
Dox concentration (ng/ml)

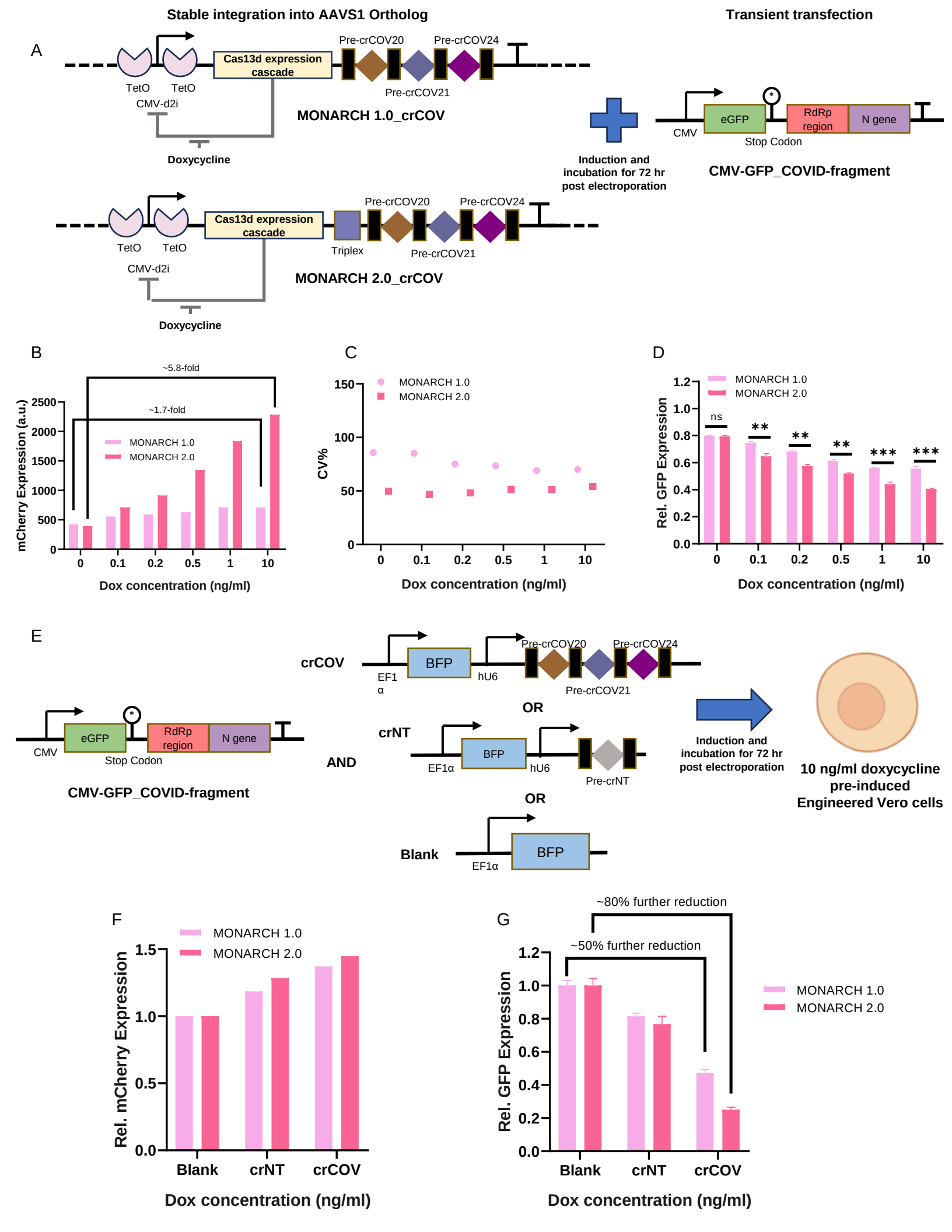
Stable integration into AAVS1 Ortholog
Transient transfection
A
TetO
TetO
CMV-d2i
Cas13d expression cascade
Pre-crCOV20
Pre-crCOV24
Pre-crCOV21
MONARCH 1.0_crCOV
Doxycycline
Induction and incubation for 72 hr post electroporation
CMV
eGFP
RdRp region
N gene
Stop Codon
CMV-GFP_COVID-fragment
Triplex
MONARCH 2.0_crCOV
B
~5.8-fold
~1.7-fold
MONARCH 1.0
MONARCH 2.0
mCherry Expression (a.u.)
Dox concentration (ng/ml)
C
CV%
D
Rel. GFP Expression
ns
E
crCOV
BFP
EF1 α
hU6
OR
crNT
Pre-crNT
AND
Blank
EF1α
10 ng/ml doxycycline pre-induced Engineered Vero cells
F
Rel. mCherry Expression
Blank
crNT
crCOV
G
~80% further reduction
~50% further reduction